

Towards a full quantitative description of single-molecule reaction kinetics in biological cells

Denis S. Grebenkov,^{1,*} Ralf Metzler,^{2,†} and Gleb Oshanin^{3,‡}

¹*Laboratoire de Physique de la Matière Condensée (UMR 7643),*

CNRS – Ecole Polytechnique, University Paris-Saclay, 91128 Palaiseau, France

²*Institute of Physics & Astronomy, University of Potsdam, 14476 Potsdam-Golm, Germany*

³*Sorbonne Université, CNRS, Laboratoire de Physique Théorique de la Matière*

Condensée (UMR CNRS 7600), 4 Place Jussieu, F-75005, Paris, France

(Dated: November 29, 2018)

The first-passage time (FPT), i.e., the moment when a stochastic process reaches a given threshold value for the first time, is a fundamental mathematical concept with immediate applications. In particular, it quantifies the statistics of instances when biomolecules in a biological cell reach their specific binding sites and trigger cellular regulation. Typically, the first-passage properties are given in terms of mean first-passage times. However, modern experiments now monitor single-molecular binding-processes in living cells and thus provide access to the full statistics of the underlying first-passage events, in particular, inherent cell-to-cell fluctuations. We here present a robust explicit approach for obtaining the distribution of FPTs to a small partially-reactive target in cylindrical-annulus domains, which represent typical bacterial and neuronal cell shapes. We investigate various asymptotic behaviours of this FPT distribution and show that it typically is very broad in many biological situations: thus, the mean FPT can differ from the most probable FPT by orders of magnitude. The most probable FPT is shown to strongly depend only on the starting position within the geometry and to be almost independent of the target size and reactivity. These findings demonstrate the dramatic relevance of knowing the full distribution of FPTs and thus open new perspectives for a more reliable description of many intracellular processes initiated by the arrival of one or few biomolecules to a small, spatially localised region inside the cell.

Keywords: First passage time distribution — Mean and most probable first passage times — Reactive boundary condition — Self-consistent approximation

I. INTRODUCTION

Many intracellular processes of signalling, regulation, infection, immune reactions, metabolism, or transmitter release in neurons are triggered by the arrival of one or few biomolecules to a small spatially localised region [1, 2]. Such processes determine the cellular function and are controlled by the statistics of the first-passage time (FPT) to a reaction event (also called the reaction time), i.e., the instant in time when the respective molecules hit their target site for the first time and initiate biochemical responses [3–8]. With modern techniques such as superresolution microscopy, it is possible to monitor individual, single-molecular biochemical regulation and production processes in living cells, revealing, for instance, pronounced fluctuations of production events of individual messenger RNA or proteins within a single cell as well as striking differences of production patterns between genetically identical cells [9–11].

Most available analytical results to quantify the first-passage dynamics were obtained for the *mean* first-passage time (MFPT) [12–30], corresponding to the inverse of the mean rate constant conventionally used in

biochemistry. For a bounded domain the MFPT is typically proportional to the domain volume, and it diverges as the target region shrinks. In particular, for the so-called narrow escape problem, which pertains to a variety of situations when a diffusive particle has to leave a bounded domain through a very small window on its boundary [30, 31], the MFPT determines the characteristic decay time of the exponential right tail of the distribution of the FPT, likewise, for the case of a small target inside bounded circular domains [32, 33]. This signifies that the MFPT is dominated by rather rare, anomalously long searching trajectories, and thus can be non-representative of the actual behaviour, or, at least be not the only important characteristic time-scale. Indeed, if a particle with diffusion coefficient D is released within a short distance δ to the target, the relevant time scale would be δ^2/D , whereas the MFPT would be of the order of L^2/D , where L is the size of the domain. As a consequence, in this case the kinetics of the aforementioned biological processes will most likely be determined by the most probable FPT, which can be orders of magnitude smaller than the MFPT, a scenario recently called the few-encounter limit [32]. Moreover, it was shown that two FPT events in the same system may be dramatically disparate [34–36]. In these common and biologically relevant situations, the whole FPT distribution is needed to adequately quantify the molecular process and to meaningfully extract the kinetic parameters from measurements.

*Electronic address: denis.grebenkov@polytechnique.edu

†Electronic address: rmetzler@uni-potsdam.de

‡Electronic address: oshanin@lptmc.jussieu.fr

However, the exact FPT distribution is known only for few elementary cases such as the FPT to a perfectly reactive target placed at the centre of a spherical region or to its boundary, starting from a fixed location [3]. At the same time, already finding the distribution of FPTs to a small target region on the otherwise reflecting boundary of a sphere remains an open problem. To our knowledge, the only nontrivial case, for which an exact FPT distribution was recently derived, is that of an arc-shaped target on the boundary of a disk [39]. To study the FPT in more complicated realistic geometries, some approximate techniques have been developed, such as the uniform approximation [40] and the asymptotically exact Newton-series approach [32]. Otherwise, one resorts to the numerical analysis of the full FPT distribution [41]. We emphasise that an impact of a finite reactivity on the form of the FPT distribution remains a completely open question.

We here report the approximate, but explicit and very accurate expression for the distribution of the FPT to a partially-reactive annular target on a cylinder, surrounded by a larger impermeable cylinder and capped by two parallel planes (Fig. 1), which is the relevant geometry to describe the first passage of molecules to the nucleoid region of bacteria cells or to a central filament trail in the axon of a neuronal cell. Another example of such a geometry is provided by a usual experimental set-up for the analysis of a diffusive search by a transcription factor protein for a specific binding site on a single strand of elongated DNA (inner cylinder), with the outer cylinder being the wall of the container. We also note that from a mathematical point of view, the method underlying the derivation of this FPT distribution can be formally generalised to arbitrary bounded domains with a small target region, and thus become applicable to the narrow escape problem in presence of a barrier at the escape window.

Our solution relies on the self-consistent approximation (SCA) technique originally devised by Shoup, Lipari, and Szabo [37] for the analysis of reaction rates between particles with inhomogeneous reactivity, and recently applied to the MFPT in spherical [28] and cylindrical geometries [38]. Within this approximation, the exact mixed boundary condition is replaced by an effective one, reducing the problem to finding self-consistent solutions. We adapt this approximation to the modified Helmholtz equation governing the survival probability in Laplace domain and thus the FPT distribution, which is subsequently checked against the numerical solution of the original problem, and is shown to be in a remarkable agreement with the latter. We note that the symmetries of the geometry under study permit us to express the FPT distribution in a compact form under rather general conditions: for arbitrary radii of the inner and the outer cylinders, for arbitrary starting points, fixed or averaged over the volume or over the cylindrical surface of a given radius, and for an arbitrary chemical reactivity κ defining the probability of a reaction with the target upon encounter.

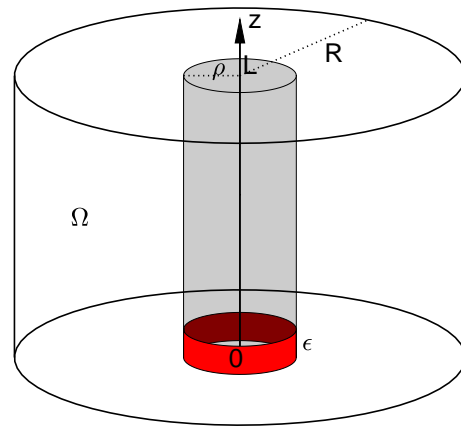


FIG. 1: Schematic presentation of the cylindrical-annulus domain Ω between two concentric cylinders of radii ρ and R and capped by planes at $z = 0$ and $z = L$. The target region is the red annulus of radius ρ and height ϵ .

We illustrate various features of this distribution, e.g., its progressive broadening as the outer cylinder is becoming larger, or the size of the target region is getting smaller, and highlight the relevance of the most probable FPT. In addition, our analysis unveils remarkable effects of the chemical reactivity κ on the functional shape of the FPT distribution which were not studied systematically before (Fig. 2). In particular, we proceed to show that upon lowering κ , a plateau-like region develops beyond the most probable FPT, such that, interestingly, the values of the FPT in an interval ranging over several decades turn out to be almost equally probable (see Fig. 5). Moreover, the chosen shape of a capped cylindrical annulus allows us to explore various features of *effectively* one- (semi-infinite cylindrical annulus), two- (exterior of a capped cylinder), and three-dimensional (exterior of a semi-infinite cylinder) search in unbounded domains, for which the MFPT is infinite. In particular, we recover the characteristic right tails $t^{-3/2}$ and $1/(t \ln^2 t)$ of the FPT distribution in effectively one- and two-dimensional geometries [3]. Therefore, our analysis also provides a seminal unifying framework in which the behaviour specific to one-, two- and three-dimensional unbounded systems appears in particular limits. Overall, our results emphasise an absolute necessity of studying the first passage phenomena in biologically relevant systems beyond the MFPT and mean rates, and show that the knowledge of the full FPT distribution is indeed indispensable for getting a complete understanding of the wealth of kinetic behaviour in such systems.

II. RESULTS

We study the distribution of the FPT to an annular reactive region Γ (the target site) on a cylinder of radius ρ when diffusion is restricted by an outer, concentric

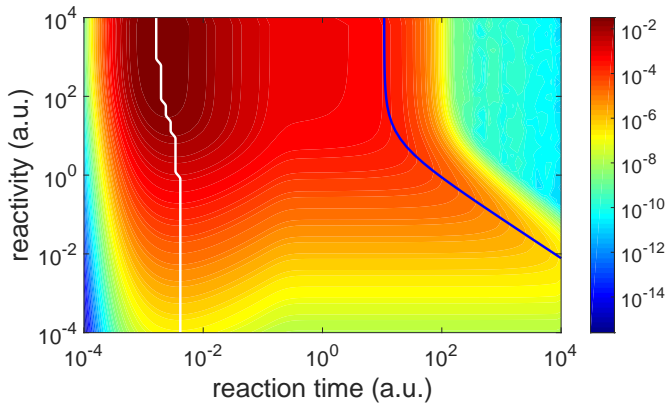


FIG. 2: Impact of the finite reactivity onto the FPT probability density (shown as a “heatmap”, in which the value of the FPT density is determined by the colour code). When the reactivity decreases, the distribution becomes much broader and extends toward longer reaction times. Blue and white curves show respectively the mean and the most probable FPTs versus the reactivity, and differ by orders of magnitude. The FPT probability density was obtained via a numerical Laplace inversion of the solution (7).

and impermeable cylinder of radius R (Fig. 1). In other words, diffusion occurs within the confining cylindrical-annulus domain Ω spanned by the interval $z \in (0, L)$ along the cylinder axis and the radius $r = \sqrt{x^2 + y^2}$ in the interval $r \in (\rho, R)$. The target consists of the annular domain Γ on the inner cylinder, specified by the interval $z \in (0, \epsilon)$ along the cylinder axis and the radius $r = \rho$. Note that the cylindrical domain is capped by reflecting planes at $z = 0$ and $z = L$ so that the scenario is in fact equivalent to diffusion in an infinite cylinder with a periodic arrangement of targets. For a particle seeded at some point $\mathbf{x} \in \Omega$, the survival probability $S(\mathbf{x}, t) = \int_{\Omega} P(\mathbf{x}, \mathbf{x}', t) d\mathbf{x}'$ is calculated as the volume integral of the (non-normalised) density function $P(\mathbf{x}, \mathbf{x}', t)$ to find the particle at position \mathbf{x}' at time t . The derivative of the survival probability with respect to time, taken with sign minus, then produces the probability density of first passage time, $H(\mathbf{x}, t) = -\partial S(\mathbf{x}, t)/\partial t$. In Laplace domain, defined in terms of $\tilde{f}(p) = \int_0^\infty \exp(-pt)f(t)dt$, this relation can be rewritten as $\tilde{H}(\mathbf{x}, p) = 1 - p\tilde{S}(\mathbf{x}, p)$, where we used the initial condition $S(\mathbf{x}, t = 0) = 1$, that is, initially the particle is present in the domain Ω with unit probability.

The survival probability, written in cylindrical coordinates (r, z, φ) , satisfies the backward Fokker-Planck equation $\partial S(\mathbf{x}, t)/\partial t = D\Delta S$, where D is the bulk diffusion coefficient, and $\Delta = \partial_r^2 + r^{-1}\partial_r + \partial_z^2 + r^{-2}\partial_\varphi^2$ is the Laplace operator. In Laplace domain, this equation reduces to the modified Helmholtz equation

$$(p - D\Delta)\tilde{S}(\mathbf{x}, p) = 1. \quad (1)$$

Due to the axial symmetry of the problem, there is no

dependence on the polar angle φ . The reflecting boundary conditions at the outer boundaries are taken into account by setting the derivatives $\partial S/\partial r = 0$ at $r = R$ and $\partial S/\partial z = 0$ at $z = 0, L$, respectively. To simplify notations, we replace the axial coordinate z by $\theta = \pi z/L$, and introduce $\epsilon = \pi\epsilon/L$. The mixed boundary condition on the inner cylinder then reads

$$D(\partial\tilde{S}/\partial r)_{r=\rho} = \begin{cases} \kappa\tilde{S}_{r=\rho} & (0 < \theta < \epsilon) \\ 0 & (\epsilon < \theta < \pi) \end{cases} \quad (2)$$

in Laplace domain. The reactivity coefficient κ in the Robin boundary condition determines the degree of stickiness of the reactive boundary Γ and is associated with the probability of the reaction with the target upon an encounter [42–44]. In standard terms, κ (in units m/s) is defined as the rate describing the number of reaction acts per unit of time within the volume of the reaction zone around Γ , times the reaction radius and hence, is a material property independent of ϵ (see [45] for more details). For a non-reactive target one has $\kappa = 0$, while $\kappa = \infty$ corresponds to the case of a perfect reaction which, on encounter, occurs with probability 1. We note that the effect of κ on the shape of the full distribution of the FPT is a novel feature here. The only available previous analysis concerned solely its effect on the MFPT, and showed that in related settings it can indeed be decisive [28, 38]. This naturally raises the question of the effects of a finite reactivity beyond the MFPT.

We apply a SCA by replacing the mixed boundary condition (2) by the inhomogeneous Neumann condition [37]

$$D(\partial\tilde{S}/\partial r)_{r=\rho} = Q\Theta(\epsilon - \theta), \quad (3)$$

in which $\Theta(z)$ is the Heaviside step function and the effective flux Q remains to be determined by imposing an appropriate self-consistent closure relation [37], i.e., by requiring that the first line in (2) holds on average, i.e., $D \int_0^\epsilon d\theta (\partial\tilde{S}/\partial r)_{r=\rho} = \kappa \int_0^\epsilon d\theta \tilde{S}_{r=\rho}$.

We search a solution in the generic form

$$\tilde{S}(r, \theta; p) = \frac{R^2}{D} \left(u_0(r) + \sum_{n=0}^{\infty} a_n g_n(r) \cos n\theta \right), \quad (4)$$

where the first term is the solution of the inhomogeneous problem with Dirichlet boundary condition at $r = \rho$, a_n are unknown coefficients to be determined, and $g_n(r)$ are radial functions satisfying the ordinary differential equation

$$g_n'' + \frac{1}{r}g_n' - \left(\frac{\pi^2 n^2}{L^2} + \frac{s}{R^2} \right) g_n = 0, \quad (5)$$

where the prime denotes radial derivative and $s = pR^2/D$ is the dimensionless Laplace variable. We emphasise the dependence of $u_0(r)$, a_n and $g_n(r)$ on the Laplace variable, although we do not write it explicitly for the sake of brevity.

The solution of (5) satisfying the boundary condition $(\partial g_n / \partial r)_{r=R} = 0$ is a linear combination of modified Bessel functions $I_n(z)$ and $K_n(z)$ of first and second kind,

$$g_n(r) = I_0(\alpha_n r/L)K_1(\alpha_n R/L) + K_0(\alpha_n r/L)I_1(\alpha_n R/L), \quad (6)$$

with $\alpha_n = \sqrt{\pi^2 n^2 + sL^2/R^2}$. The solution of the inhomogeneous problem with Dirichlet boundary condition at $r = \rho$ reads $u_0(r) = [1 - g_0(r)/g_0(\rho)]/s$ [3, 46]. The coefficients a_n are determined in the Supplemental Information (SI), section I, and we obtain the final result for the FPT density

$$\tilde{H}(r, \theta; p) = \eta \frac{g_0(r)}{g_0(\rho)} + 2\eta \frac{g'_0(\rho)}{g_0(\rho)} \sum_{n=1}^{\infty} \frac{g_n(r)}{g'_n(\rho)} \frac{\sin n\varepsilon}{n\varepsilon} \cos(n\theta), \quad (7)$$

in Laplace domain, where

$$\eta = \left(1 - \left(\frac{\pi D}{\kappa\varepsilon} + \frac{L}{\pi} \mathcal{R}_\varepsilon\right) \frac{g'_0(\rho)}{g_0(\rho)}\right)^{-1} \quad (8)$$

and

$$\mathcal{R}_\varepsilon = -\frac{2\pi}{L} \sum_{n=1}^{\infty} \frac{g_n(\rho)}{g'_n(\rho)} \left(\frac{\sin n\varepsilon}{n\varepsilon}\right)^2. \quad (9)$$

This approximate representation of the FPT density in the cylindrical-annulus domain is one of the main results of this paper. This result hinges on the SCA, which has already been applied for the analysis of the MFPT in spherical [28] and cylindrical-annulus [38] geometries, and verified against the numerical solution of the mixed boundary problem. Moreover, a similar SCA approach has been used in [45] to calculate the self-propulsion velocity of catalytically-active colloids and was shown to be in very good agreement with already known results, only slightly underestimating some insignificant numerical factors. In Sec. II of the SI we show that it is a remarkably accurate approximation for the problem under study, checking it for different initial conditions against the numerical solution of the original mixed boundary value problem.

The moments of this FPT distribution can be obtained from $\tilde{H}(r, \theta; p)$ in the form $T_n = (-1)^n \lim_{p \rightarrow 0} (\partial^n / \partial p^n) \tilde{H}(r, \theta; p)$. The first moment T_1 is the mean FPT that we also denote as T for brevity. The explicit solution in (7) fully determines the statistics of the FPT. Since $\tilde{S}(r, \theta; p)$ and the FPT density $\tilde{H}(r, \theta; p)$ are trivially related in Laplace domain, we focus on the latter quantity, bearing in mind that all properties of the Laplace-transformed survival probability follow immediately from those of $\tilde{H}(r, \theta; p)$. The inverse Laplace transform can be performed either by determining the poles of $\tilde{H}(r, \theta; p)$ and using the residue theorem, or by numerical inversion using the Talbot algorithm. In Sec. III of the SI, we discuss in more detail the former approach, whereas the numerical inversion is used throughout the paper. The solutions in

the limiting cases $R \rightarrow \infty$ and $L \rightarrow \infty$ are presented in the SI (Sections VI and VII).

As already remarked, we will consider different situations with respect to the starting point of the particle. If the starting point is distributed uniformly in the bulk, the volume average of $\tilde{H}(r, \theta; p)$ can be evaluated exactly,

$$\overline{\tilde{H}(p)} = 2 \int_0^\pi d\theta \int_\rho^R \frac{dr r \tilde{H}(r, \theta; p)}{\pi(R^2 - \rho^2)} = \frac{-2\rho g'_0(\rho)\eta}{s(1 - \rho^2/R^2)g_0(\rho)}, \quad (10)$$

where we used the identity $\int_\rho^R dr r g_n(r) = -\rho L^2 g'_n(\rho) / \alpha_n^2$. If in turn the average is taken over uniformly distributed starting points on a cylindrical surface of radius r , we find

$$\overline{\tilde{H}(p)}_r = \frac{1}{\pi} \int_0^\pi d\theta \tilde{H}(r, \theta; p) = \eta \frac{g_0(r)}{g_0(\rho)}. \quad (11)$$

Setting $r = \rho$ (when a particle starts from the inner boundary with uniform density), this relation turns out to provide a natural interpretation for the coefficient η defined in (8).

As discussed in Ref. [46], $\tilde{H}(r, \theta; p)$ can also be interpreted as the probability that a mortal walker with bulk killing rate p reaches the target. For $p = 0$ the classical immortal walker reaches the target with unit probability because of the recurrent character of restricted Brownian motion in a bounded domain. In turn, when $p > 0$, the random walker can be killed during its search for the target, and $\tilde{H}(r, \theta; p)$ is the fraction of walkers that reach the target before being killed.

III. DISCUSSION

The explicit form of the Laplace-transformed FPT distribution $\tilde{H}(r, \theta; p)$ in (7) provides unprecedented opportunities for studying the details of the first passage dynamics in a cylindrical-annulus domain. The major challenge here is the relatively large number of relevant parameters of this problem. In fact, the short-time and the long-time behaviours of the FPT distribution (i.e., its left and right tails) strongly depend on the four geometric parameters R , L , ρ , and ε , as well as on the reactivity κ , and on the starting point (in particular, whether it is fixed or randomly distributed over some subspace). For instance, the behaviour in the small-target limit $\varepsilon \rightarrow 0$ is expected to be different from that in the thin cylinder limit $\rho \rightarrow 0$. Moreover, one can also investigate the limiting cases of the unbounded exterior of a capped cylinder ($R \rightarrow \infty$), and of an infinitely long cylinder ($L \rightarrow \infty$). In these two limits, the distribution of the FPTs remains well defined, although the MFPT is infinite, as shown in Sections VI and VII of the SI. We discuss below the various facets of the FPT distribution in different parameter ranges as well as some direct applications.

A. General qualitative behaviour

The form of the left tail of the FPT distribution (corresponding to short FPTs) strongly depends on the starting point of the particle. If the starting point is fixed (or surface-averaged with $r > \rho$), the FPTs are dominated by very rare trajectories from \mathbf{x} to the closest points of the target (called direct trajectories in Refs. [32, 33]). As $t \rightarrow 0$, we thus expect the behaviour $H(\mathbf{x}, t) \propto \exp(-|\mathbf{x} - \Gamma|/[4Dt])$, where $|\mathbf{x} - \Gamma|$ is the Euclidean distance between the starting point \mathbf{x} and the target domain Γ . In this limit, the FPT density vanishes very rapidly, meaning that very short FPTs are extremely unlikely. In turn, if the starting point is averaged over the volume or over the inner surface at $r = \rho$, such that some particles are initially released right at the surface of the target, one can expect that the FPT density is peaked at $t = 0$ and then monotonically decreases with t . In this case, an intermediate power law decay of the FPT distribution is expected. In particular, the general asymptotic behaviour derived in Ref. [46] for the perfectly reactive target implies $\overline{H(p)} \simeq (|\Gamma|/|\Omega|) (p/D)^{-1/2}$, thus

$$\overline{H(t)} \simeq (2\rho\varepsilon D)\pi^{-3/2}(R^2 - \rho^2)^{-1}(Dt)^{-1/2} \quad (12)$$

as $t \rightarrow 0$. In the partially reactive case $\kappa < \infty$ the intermediate power-law decay has a different form, see Sec. III C.

The form of the right tail of the FPT distribution essentially depends on whether the domain Ω is bounded or not. For any bounded domain, the spectrum of the governing Laplace operator is discrete, and the FPT density exhibits an exponential decay whose rate is determined by the smallest non-trivial eigenvalue λ_0 : $H(\mathbf{x}, t) \propto \exp(-Dt\lambda_0)$ as $t \rightarrow \infty$. In Sec. III B we relate the decay rate to the surface-averaged MFPT \overline{T}_ρ , which is finite. The behaviour is different in the limits $R \rightarrow \infty$ or $L \rightarrow \infty$ when the domain Ω becomes unbounded. In this case, the MFPT is infinite, and the FPT density exhibits a power law decay (possibly with logarithmic corrections). We discuss this behaviour in detail in the SI (see Sections VI and VII). It is important to stress that the related power law behaviour can also be relevant even for bounded domains as an intermediate regime, before the ultimate exponential cut-off, see also the findings for spherical domains in Ref. [32–36]. As we will illustrate below, such an intermediate power law regime can spread over a quite broad range of times and thus be the most interesting feature of the underlying FPT phenomenon. In this situation, the most probable FPT can differ from the MFPT by many orders of magnitude.

B. The right-tail of the FPT distribution

In the limit $p \rightarrow 0$ the Laplace transform $\tilde{H}(r, \theta; p)$ of the FPT density determines both the moments T_n of the FPT and the long-time behaviour of $H(r, \theta; t)$ itself.

Taking the respective limits of the radial function discussed in Sec. IV of the SI, we obtain $\overline{H(t)}_\rho$ as the inverse Laplace transformation of η , namely,

$$\overline{H(t)}_\rho \simeq \exp(-t/\overline{T}_\rho)/\overline{T}_\rho, \quad (13)$$

valid for $t \rightarrow \infty$. The characteristic time is given by

$$\overline{T}_\rho = \frac{R^2 - \rho^2}{2D\rho} \left(\frac{\pi D}{\kappa\varepsilon} + \frac{L}{\pi} \mathcal{R}_\varepsilon(p=0) \right), \quad (14)$$

which corresponds to the surface-averaged MFPT investigated in Ref. [38]. This result is expected for diffusion in a bounded domain. The asymptotic behaviour of other quantities can be obtained in a similar way. For instance,

$$\overline{H(t)}_r \simeq \exp(-t/\overline{T}_r)/\overline{T}_r, \quad (15)$$

with the characteristic time

$$\overline{T}_r = \overline{T}_\rho + \left(\frac{\rho^2 - r^2}{4D} + \frac{R^2 \ln(r/R)}{2D} \right), \quad (16)$$

where the second term in the parentheses is the MFPT to the inner cylinder from a uniformly distributed point at the cylindrical surface at r . The additivity of two MFPTs reflects the fact that any trajectory from such a point to the target can be split into two independent parts: the path from the cylinder at r to the cylinder at ρ , and the path from the cylinder at ρ to the target, similar to the results for inhomogeneous diffusion in a cylindrical domain [57].

C. The left tail of the FPT distribution

The form of the left tail of the FPT distribution stems from the asymptotic behaviour of $\tilde{H}(r, \theta; p)$ in the limit $p \rightarrow \infty$. After the transformations detailed in the SI (see Section IV), we obtain the Laplace-transformed FPT density $\tilde{H}(r, \theta; p)$ along with its volume and surface averages, $\overline{H(p)}$ and $\overline{H(p)}_r$. Here one needs to distinguish the cases of perfect ($\kappa = \infty$) and imperfect ($\kappa < \infty$) reactivity at the target. Note that the difference in the asymptotic behaviours for perfectly or only partially reactive targets was discussed for other geometries in Refs. [58, 59].

1. Perfect reactions

According to (11) the inverse Laplace transform of asymptotic (S34) in the SI yields the asymptotic behaviour of the surface-averaged FPT density $\overline{H(t)}_\rho$ at small t , namely,

$$\overline{H(t)}_\rho \simeq (\varepsilon/\pi)\delta(t) + (D/[8\pi])^{1/2}L^{-1}t^{-1/2} + O(1). \quad (17)$$

The first term represents the fraction ε/π of particles, that started right at the target, for which the first passage time is zero. The next term accounts for the FPTs of

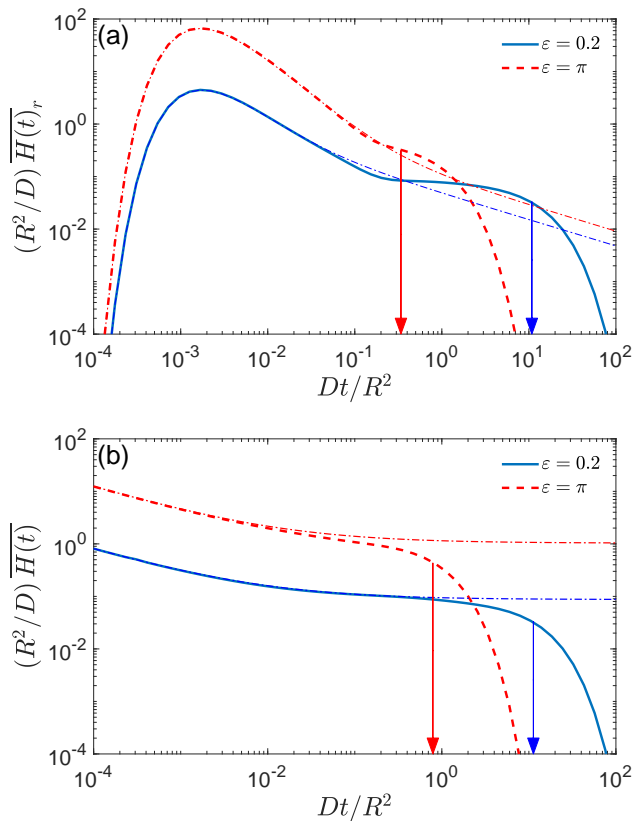


FIG. 3: Surface-averaged (a) and volume-averaged (b) FPT densities $\overline{H(t)}_r$ and $\overline{H(t)}$ as functions of t for perfect reactions ($\kappa = \infty$) with $L/R = \pi$, $\rho/R = 0.1$, $r/R = 0.2$, and $\varepsilon = 0.2$ (solid line) and $\varepsilon = \pi$ (dashed line). Both curves are obtained by the numerical Laplace inversion of (7). The two arrows indicate the MFPT $D\overline{T}_r/R^2$ for both cases: 10.82 ($\varepsilon = 0.2$) and 0.34 ($\varepsilon = \pi$) for surface-averaged quantity, and 11.27 ($\varepsilon = 0.2$) and 0.79 ($\varepsilon = \pi$) for volume-averaged quantity. Dash-dotted lines indicate the short-time asymptotic (18) and (19), and agree very well with the general result in (7) well beyond the most probable FPT. Length and time scales are fixed by setting $R = 1$ and $R^2/D = 1$.

particles with non-zero initial separations from the target. Since (S33) was derived for $\varepsilon \leq \pi/2$, the above asymptotic behaviour is not applicable for the case $\varepsilon = \pi$, for which $\overline{H(t)}_\rho = \delta(t)$ without correction terms.

When the particles start from a cylindrical surface at r , (11) has an extra factor $g_0(r)/g_0(\rho)$. With the large- p asymptotic (S36) we find the short-time behaviour

$$\overline{H(t)}_r \simeq \frac{\varepsilon}{\pi} (\rho/[4\pi r D t^3])^{1/2} \exp(-(r-\rho)^2/[4Dt]) \times \left(r - \rho + Dt \left(\frac{\pi}{\sqrt{2}L\varepsilon} + \frac{\sqrt{1/\rho} - \sqrt{1/r}}{4\sqrt{R}} \right) + O(t^2) \right). \quad (18)$$

Figure 3(a) shows the surface-averaged probability density $\overline{H(t)}_r$ for two choices of the target height: $\varepsilon = 0.2$ and $\varepsilon = \pi$. The latter case describes the whole inner cylinder as reactive, while the former value of ε is chosen

arbitrarily and meant to illustrate a moderately small target. In both cases shown in the figure the short-time asymptotic (18) is very accurate up to $Dt/R^2 \lesssim 0.1$. When the target is the entire inner cylinder ($\varepsilon = \pi$) this time scale is of the order of the corresponding MFPT $D\overline{T}_r/R^2 \approx 0.34$. For times of that order the FPT density has an exponential cut-off. For the case of a partially reactive inner cylinder ($\varepsilon = 0.2$) the MFPT is, notably, around four decades longer than the most likely FPT.

For the volume average, (10), together with S34, yields a different short-time behaviour, namely,

$$\overline{H(t)} \simeq \frac{\rho D}{R^2 - \rho^2} \left(\frac{2\varepsilon}{\pi\sqrt{\pi Dt}} + \left(\frac{1}{\sqrt{2}L} + \frac{\varepsilon}{\pi\rho} \right) + O(t^{1/2}) \right). \quad (19)$$

The leading term agrees with the general behaviour in (12). Figure 3(b) shows the FPT density obtained by numerical inversion of $\overline{H(p)}$ from (7). In the particular case $\varepsilon = \pi$ (the entire inner cylinder is absorbing), one has $a_n = 0$ and thus (7) is exact. One can see that both distributions are broad. The asymptotic (19) is remarkably accurate for both cases $\varepsilon = \pi$ and $\varepsilon = 0.2$.

2. Imperfect reactions

For imperfect reactions with finite reactivity κ the first arrival onto the target does not necessarily imply a successful reaction, so that the reaction times are increased. Indeed, for $\kappa < \infty$, (S33) in the SI acquires the asymptotic (S37), from which we get the short-time behaviours

$$\overline{H(t)}_\rho \simeq \frac{\varepsilon}{\pi} \frac{\kappa}{\sqrt{\pi Dt}} - \frac{\varepsilon}{\pi} \left(\frac{\kappa^2}{D} + \frac{\kappa}{2\rho} \right) + O(\sqrt{t}), \quad (20a)$$

$$\overline{H(t)}_r \simeq \frac{\varepsilon}{\pi} \sqrt{\rho/r} \frac{\kappa}{\sqrt{\pi Dt}} \exp\left(-\frac{(r-\rho)^2}{4Dt}\right), \quad (20b)$$

$$\overline{H(t)} \simeq \frac{2\rho\varepsilon\kappa}{\pi(R^2 - \rho^2)} \left(1 - \frac{2\kappa\sqrt{Dt}}{D\sqrt{\pi}} + O(t) \right). \quad (20c)$$

Interestingly, for imperfect reactions the leading short-time behaviour of the FPT distribution appears to be distinctly different, depending on the starting point: $\overline{H(t)}_\rho$ diverges as $t \rightarrow 0$, $\overline{H(t)}_r$ tends to zero in this limit, while $\overline{H(t)}$ approaches a constant value.

Figure 4(a) shows the surface-averaged FPT density $\overline{H(t)}_r$ at $r/R = 0.2$ and $\kappa R/D = 1$. One can see that the short-time asymptotic (20b) accurately reproduces the behaviour of this density up to its maximum. As a consequence, the position t_m of this maximum can be obtained by taking the derivative of (20b) with respect to t and setting the resulting expression equal to zero. This gives the following estimate for the most probable FPT:

$$t_m = (r - \rho)^2 / (2D). \quad (21)$$

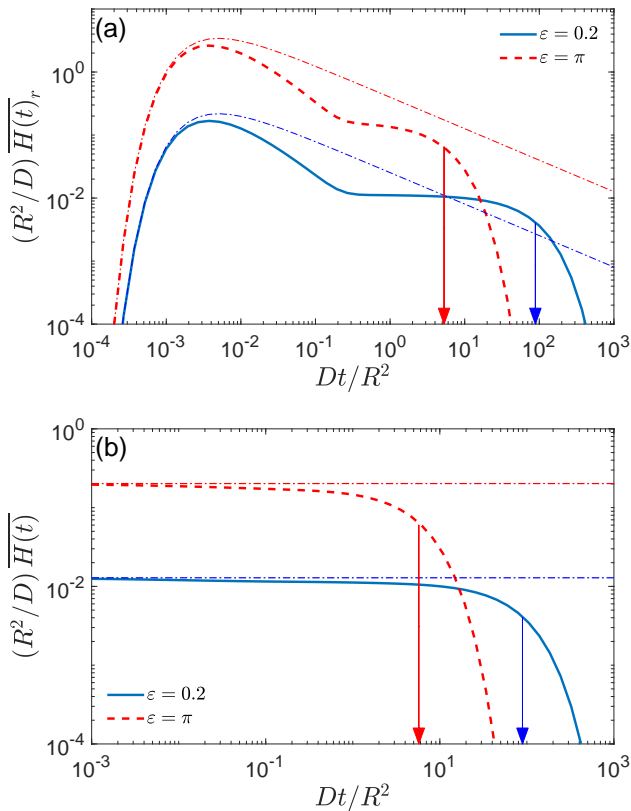


FIG. 4: Surface-averaged (a) and volume-averaged (b) FPT densities $\overline{H(t)}_r$ and $\overline{H(t)}$ as functions of t for imperfect reactions ($\kappa R/D = 1$, cf. Fig. 3), with $L/R = \pi$, $\rho/R = 0.1$, $r/R = 0.2$, and $\varepsilon = 0.2$ (solid line) and $\varepsilon = \pi$ (dashed line). Both curves are obtained by numerical Laplace inversion of (7). The two arrows indicate the MFPT $D\overline{T}_r/R^2$ for both cases: 88.58 ($\varepsilon = 0.2$) and 5.29 ($\varepsilon = \pi$) for surface-averaged quantity, and 89.03 ($\varepsilon = 0.2$) and 5.74 ($\varepsilon = \pi$) for volume-averaged quantity. Dash-dotted lines show the short-time asymptotic (20b) and (20c) (in which only the leading term is kept). Length and time scales are fixed by setting $R = 1$ and $R^2/D = 1$.

The estimated value of t_m in (21) depends only on the distance to the target but does not depend on either the target size ε or the reactivity κ , nor on the inner radius of the cylinder. In this example, $Dt_m/R^2 = 0.005$, whereas the MFPT is four orders of magnitude higher. Similar to the findings in Ref. [32] the most likely FPT corresponds to geometry-controlled, direct trajectories, in which the initial distance from the target is decisive.

We also note that the probability density is broader in the case $\varepsilon = 0.2$, with a flat intermediate region between the maximum hump and the exponential cut-off (in the region $0.2 \leq Dt/R^2 \leq 10$). As the target size ε or the reactivity κ decrease, the MFPT increases and thus the exponential cut-off moves towards longer times. In turn, the position and shape of the maximum remain approximately constant (dominated by the initial distance and the diffusivity D) so that the intermediate region ex-

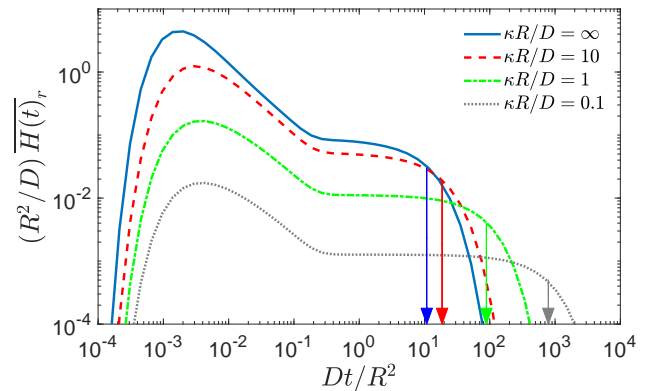


FIG. 5: Surface-averaged FPT density $\overline{H(t)}_r$ as function of t for imperfect reactions, with $L/R = \pi$, $\rho/R = 0.1$, $r/R = 0.2$, and $\varepsilon = 0.2$. All curves are obtained by numerical Laplace inversion of (7). Arrows indicate the MFPT $D\overline{T}_r/R^2$: 10.82 ($\kappa = \infty$), 18.60 ($\kappa = 10$), 88.58 ($\kappa R/D = 1$), and 788.36 ($\kappa R/D = 0.1$). Note that (at fixed D) the MFPT grows with decreasing κ . In this regime the MFPT becomes dominated by chemical reactivity, $\overline{T}_r \sim 1/\kappa$ (see Refs. [28, 38]). The most probable FPT exhibits a weak dependence on κ . Note also the appearance of a pronounced plateau-like region, which stretches over progressively longer times scales upon lowering the reactivity κ . Hence, there is a broad range of times with equiprobable realisations of the FPT. Length and time scales are fixed by setting $R = 1$ and $R^2/D = 1$.

pands, as we checked for $\varepsilon = 0.05$ and for $\kappa R/D = 0.1$ (not shown). This is a striking result: if the particle does not manage to find the target and react within short times comparable to t_m (around the maximum), it explores the entire confining domain with eventual returns to the target. As a consequence, its reaction time is distributed almost uniformly over a very broad range of times, up to the exponential cut-off which is essentially determined by the MFPT. The latter, in turn, is dominated by the chemical reactivity, while the diffusive search for the target provides only a sub-dominant contribution [38] (see also [28] for a general discussion). One can see that the low reactivity κ leads to an homogenisation of the search process, as evidenced in Fig. 5, and the plateau-like region past the most probable FPT extends over progressively longer scales when κ becomes smaller. As a consequence, the values of FPTs ranging over several orders of magnitude appear to be almost equally probable.

Figure 4(b) shows that the volume-averaged FPT density $\overline{H(t)}$ remains almost constant at short times and then has an exponential cut-off. This almost uniform behaviour at short times resembles that shown in Fig. 4(a). The only difference is that there is no maximum at short times as some particles start infinitely close to the target.

D. Biological implications

The function of biological cells to large extent relies on the passive diffusion of regulatory molecules. In particular, the expression level of any gene is controlled by the binding of transcription factor proteins. Inside the chromosome a transcription factor locates its specific binding site via facilitated diffusion combining volume search with one-dimensional sliding along the DNA, as well as intersegmental jumps [47–49]. As many bacteria cells such as the well studied *E.coli* or *bacilli* have distinct cylindrical shapes, the analysis here provides an answer to the question how fast a given transcription factor can reach the chromosome from the cytoplasm of the cell in the first place. Our results demonstrate that for all considered scenarios the FPT to the nucleoid is broadly distributed and may deviate significantly from the respective MFPT. For reliable regulation it may thus be advantageous that transcription factors, which often occur in very low copy numbers in a cell, are inhomogeneously distributed in the cell [50, 51], and may thus be kept close to their target site on the DNA. This reasoning is in accord with results for the downstream gene regulation model in [52] supporting the rapid search hypothesis [53] as well as the geometry controlled few-encounter scenario of [32].

We also mention another relevant system for the cylindrical geometry, namely, axons, the up to a meter long protrusions of neuronal cells, whose diameter may span from $0.1\ \mu\text{m}$ up to $20\ \mu\text{m}$ [54]. In the giant squid the diameter may even reach the macroscopic size of 1 mm. In such an axon motor proteins detach from the central bundle of microtubules, along which the motors actively transport cargo. The motors' reattachment dynamics after unbinding, governed by the results derived herein for imperfect reactions, have shown to be important for the observed Lévy walk transport [55].

IV. CONCLUSION

Although the necessity of knowing the full FPT distribution, especially in situations when several length scales are involved, has been emphasised earlier (e.g., in [7, 8, 32, 33]), not much progress has been achieved in this direction. For the first time, we discuss here, using an analytical solution, the forms of the full first-passage time distribution for different initial conditions in a cylindrical-annulus geometry relevant for bacteria cells and neuronal axons. Due to the quite large number of parameters in the system, the full distribution of the FPT has a complicated structure and appreciably changes its shape when the parameters are changed. It would therefore be naive to expect that the full complexity of the behaviour in the system could be exhaustively

characterised by just the first moment of this distribution – the mean first-passage time – on which the previous research has concentrated almost exclusively.

Within a self-consistent approach, proposed originally in a completely different context in [37], we found explicit, approximate expressions for the full FPT distribution, which we validated by extensive numerical analysis. One of the main features that we uncovered is that, indeed, the full distribution has an important structure and is rather sensitive to a slight variation of the system's parameters. Next, we showed that the MFPT turns out to be several orders of magnitude longer than the most likely FPT, the decisive quantity indicating when typically the first molecule arrives at the target and triggers biochemical followup reactions. Therefore, while the knowledge of the MFPT is certainly helpful and important, it carries the danger of being misleading, given that the MFPT largely overestimates the typical time scales involved in cellular processes. In this context, former theoretical works devoted to the minimisation of the MFPT do not necessarily reveal the optimal conditions for the function of biological systems, because they do not affect the most likely FPT.

Equally significant result of our analysis is the occurrence of an extended plateau of the FPT distribution for lower reactivity constants κ , signifying that over more than a decade all FPTs within this range become equally probable and thus the triggering events even more unfocused. Moreover, within the unique geometric setting, we could unveil intriguing dimensionality features of the diffusive search in unbounded domains, for which the MFPT is infinite and thus useless. The derived asymptotic formulas correctly describe intermediate regimes of the FPT distribution in the bounded case as well.

Having available expressions for the full FPT distribution will allow a more faithful evaluation of measured reaction dynamics but also the planning of new experiments, in particular, when single molecule resolution is accessible. We expect that our results will lead to a new level of quantitative understanding of molecular regulation processes on microscopic levels, for instance, a renormalisation of rate constants extracted from MFPT interpretations.

Acknowledgments

DSG acknowledges the support under Grant No. ANR-13-JSV5-0006-01 of the French National Research Agency. RM acknowledges support from the Deutsche Forschungsgemeinschaft through projects ME 1535/6-1 and ME 1535/7-1, as well as from the Foundation for Polish Science within an Alexander von Humboldt Polish Honorary Research Fellowship is gratefully acknowledged.

-
- [1] B. Alberts, A. Johnson, J. Lewis, D. Morgan, M. Raff, K. Roberts, and P. Walter, *Molecular Biology of the Cell* (Garland Science, New York, NY, 2014).
- [2] D. P. Snustad and M. J. Simmons, *Principles of Genetics* (Wiley, New York, 2000).
- [3] S. Redner, *A Guide to First Passage Processes* (Cambridge, Cambridge University press, 2001).
- [4] R. Metzler, G. Oshanin, and S. Redner, *First-Passage Phenomena and Their Applications* (Singapore, World Scientific, 2014).
- [5] D. Holcman and Z. Schuss, Control of flux by narrow passages and hidden targets in cellular biology, *Phys. Progr. Rep.* **76**, 074601 (2013).
- [6] P. C. Bressloff and J. M. Newby, Stochastic models of intracellular transport, *Rev. Mod. Phys.* **85**, 135-196 (2013).
- [7] O. Bénichou, C. Loverdo, M. Moreau and R. Voituriez, Intermittent search strategies, *Rev. Mod. Phys.* **83**, 81 (2011).
- [8] O. Bénichou and R. Voituriez, From first-passage times of random walks in confinement to geometry-controlled kinetics, *Phys. Rep.* **539**, 225-284 (2014).
- [9] J. Yu, J. Xiao, X. Ren, K. Lao, and X. S. Xie, Probing Gene Expression in Live Cells, One Protein Molecule at a Time, *Science* **311**, 1600 (2006).
- [10] G.-W. Li and X. S. Xie, Central dogma at the single-molecule level in living cells, *Nature* **475**, 308 (2011).
- [11] A. Raj and A. van Oudenaarden, Nature, Nurture, or Chance: Stochastic Gene Expression and Its Consequences, *Cell* **135**, 216 (2008).
- [12] M. J. Ward and J. B. Keller, Strong Localized Perturbations of Eigenvalue Problems, *SIAM J. Appl. Math.* **53**, 770-798 (1993).
- [13] I. V. Grigoriev, Y. A. Makhnovskii, A. M. Bereshkovskii, and V. Y. Zitserman, Kinetics of escape through a small hole, *J. Chem. Phys.* **116**, 9574 (2002).
- [14] A. Singer, Z. Schuss, D. Holcman, and R. S. Eisenberg, Narrow Escape, Part I, *J. Stat. Phys.* **122**, 437-463 (2006).
- [15] A. Singer, Z. Schuss, and D. Holcman, Narrow Escape, Part II The circular disk, *J. Stat. Phys.* **122**, 465-489 (2006).
- [16] A. Singer, Z. Schuss, and D. Holcman, Narrow Escape, Part III Riemann surfaces and non-smooth domains, *J. Stat. Phys.* **122**, 491-509 (2006).
- [17] S. Condamin, O. Bénichou, V. Tejedor, R. Voituriez, and J. Klafter, First-passage time in complex scale-invariant media, *Nature* **450**, 77 (2007).
- [18] O. Bénichou and R. Voituriez, Narrow-Escape Time Problem: Time Needed for a Particle to Exit a Confining Domain through a Small Window, *Phys. Rev. Lett.* **100**, 168105 (2008).
- [19] S. Pillay, M. J. Ward, A. Peirce, and T. Kolokolnikov, An Asymptotic Analysis of the Mean First Passage Time for Narrow Escape Problems: Part I: Two-Dimensional Domains, *SIAM Multi. Model. Simul.* **8**, 803-835 (2010).
- [20] A. F. Cheviakov, M. J. Ward, and R. Straube, An Asymptotic Analysis of the Mean First Passage Time for Narrow Escape Problems: Part II: The Sphere, *SIAM Multi. Model. Simul.* **8**, 836-870 (2010).
- [21] G. Oshanin, M. Tamm, and O. Vasilyev, Narrow-escape times for diffusion in microdomains with a particle-surface affinity: Mean-field results, *J. Chem. Phys.* **132**, 235101 (2010).
- [22] A. F. Cheviakov, A. S. Reimer, and M. J. Ward, Mathematical modeling and numerical computation of narrow escape problems, *Phys. Rev. E* **85**, 021131 (2012).
- [23] C. Caginalp and X. Chen, Analytical and Numerical Results for an Escape Problem, *Arch. Rational. Mech. Anal.* **203**, 329-342 (2012).
- [24] A. M. Berezhkovskii and L. Dagdug, Effect of binding on escape from cavity through narrow tunnel, *J. Chem. Phys.* **136**, 124110 (2012).
- [25] A. M. Berezhkovskii and A. V. Barzykin, Search for a small hole in a cavity wall by intermittent bulk and surface diffusion, *J. Chem. Phys.* **136**, 054115 (2012).
- [26] D. S. Grebenkov, Universal formula for the mean first passage time in planar domains, *Phys. Rev. Lett.* **117**, 260201 (2016).
- [27] T. Guérin, N. Levernier, O. Bénichou, and R. Voituriez, Mean first-passage times of non-Markovian random walkers in confinement, *Nature* **534**, 356-359 (2016).
- [28] D. S. Grebenkov and G. Oshanin, Diffusive escape through a narrow opening: new insights into a classic problem, *Phys. Chem. Chem. Phys.* **19**, 2723-2739 (2017).
- [29] T. Agranov and B. Meerson, Narrow escape of interacting diffusing particles, *Phys. Rev. Lett.* **120**, 120601 (2018).
- [30] D. Holcman and Z. Schuss, The Narrow Escape Problem, *SIAM Rev.* **56**, 213-257 (2014).
- [31] Z. Schuss, A. Singer, and D. Holcman, The narrow escape problem for diffusion in cellular microdomains, *Proc. Nat. Acad. Sci. USA* **104**, 16098-16103 (2007).
- [32] A. Godec and R. Metzler, Universal Proximity Effect in Target Search Kinetics in the Few-Encounter Limit, *Phys. Rev. X* **6**, 041037 (2016).
- [33] A. Godec and R. Metzler, First passage time distribution in heterogeneity controlled kinetics: going beyond the mean first passage time, *Sci. Rep.* **6**, 20349 (2016).
- [34] C. Mejía-Monasterio, G. Oshanin, and G. Schehr, First passages for a search by a swarm of independent random searchers, *J. Stat. Mech.* P06022 (2011).
- [35] T. Mattos, C. Mejía-Monasterio, R. Metzler, and G. Oshanin, First passages in bounded domains: When is the mean first passage time meaningful?, *Phys. Rev. E* **86**, 031143 (2012).
- [36] T. Mattos, C. Mejía-Monasterio, R. Metzler, G. Oshanin, and G. Schehr, Trajectory-to-trajectory fluctuations in first-passage phenomena in bounded domains, in Ref. [4].
- [37] D. Shoup, G. Lipari and A. Szabo, *Biophys. J.* **36**, 697 (1981).
- [38] D. S. Grebenkov, R. Metzler, and G. Oshanin, Effects of the target aspect ratio and intrinsic reactivity onto diffusive search in bounded domains, *New J. Phys.* **19**, 103025 (2017).
- [39] J.-F. Rupprecht, O. Bénichou, D. S. Grebenkov, and R. Voituriez, Exit time distribution in spherically symmetric two-dimensional domains, *J. Stat. Phys.* **158**, 192-230 (2015).
- [40] S. A. Isaacson and J. Newby, Uniform asymptotic approximation of diffusion to a small target, *Phys. Rev. E* **88**, 012820 (2013).

- [41] A. E. Hafner and H. Rieger, Spatial cytoskeleton organization supports targeted intracellular transport, *Biophys. J.* **114**,1420-1432 (2018).
- [42] D. S. Grebenkov, M. Filoche, B. Sapoval, Spectral Properties of the Brownian Self-Transport Operator, *Eur. Phys. J. B* **36** (2), 221-231 (2003).
- [43] D. S. Grebenkov, Partially Reflected Brownian Motion: A Stochastic Approach to Transport Phenomena, in "Focus on Probability Theory", Ed. L. R. Velle, pp. 135-169 (Nova Science Publishers, 2006).
- [44] D. S. Grebenkov, Residence times and other functionals of reflected Brownian motion, *Phys. Rev. E* **76**, 041139 (2007).
- [45] G. Oshanin, M. N. Popescu and S. Dietrich, Active colloids in the context of chemical kinetics, *J. Phys. A: Math. Theor.* **50** 134001 (2017).
- [46] D. S. Grebenkov and J.-F. Rupprecht, The escape problem for mortal walkers, *J. Chem. Phys.* **146**, 084106 (2017).
- [47] P. H. von Hippel and O. G. Berg, Facilitated target location in biological systems, *J. Biol. Chem.* **264**, 675-678 (1989).
- [48] J. Elf, G. W. Li, and X. S. Xie, Probing transcription factor dynamics at the single-molecule level in a living cell, *Science* **316**, 1191-1194 (2007).
- [49] M. A. Lomholt, B. v. d. Broek, S.-M. J. Kalisch, G. J. L. Wuite, and R. Metzler, Facilitated diffusion with DNA coiling, *Proc. Natl. Acad. Sci. USA* **106**, 8204 (2009).
- [50] F. Képès, Periodic transcriptional organization of the E.coli genome, *J. Mol. Biol.* **340**, 957-964 (2004).
- [51] T. E. Kuhlman and E. C. Cox, Gene location and DNA density determine transcription factor distributions in *Escherichia coli*, *Mol. Syst. Biol.* **8**, 610 (2012).
- [52] O. Pulkkinen and R. Metzler, Distance matters: the impact of gene proximity in bacterial gene regulation, *Phys. Rev. Lett.* **110**, 198101 (2013).
- [53] G. Kolesov, Z. Wunderlich, O. N. Laikova, M. S. Gelfand, and L. A. Mirny, How gene order is influenced by the biophysics of transcription regulation, *Proc. Natl. Acad. Sci. USA* **104**, 13948 (2007).
- [54] L. Squire, *Fundamental neuroscience* (Academic Press, Amsterdam, 2013).
- [55] K. Chen, B. Wang, and S. Granick, Memoryless self-reinforcing directionality in endosomal active transport within living cells, *Nat. Mater.* **14**, 589-593 (2015).
- [56] P. Levitz, M. Zinsmeister, P. Davidson, D. Constantin, and O. Poncelet, Intermittent Brownian dynamics over a rigid strand: Heavily tailed relocation statistics, *Phys. Rev. E* **78**, 030102(R) (2008).
- [57] A. Godec and R. Metzler, Optimization and universality of Brownian search in a basic model of quenched heterogeneous media, *Phys. Rev. E* **91**, 052134 (2015).
- [58] D. S. Grebenkov, Subdiffusion in a bounded domain with a partially absorbing-reflecting boundary, *Phys. Rev. E* **81**, 021128 (2010).
- [59] D. S. Grebenkov, Searching for partially reactive sites: Analytical results for spherical targets, *J. Chem. Phys.* **132**, 034104 (2010).
- [60] H. S. Carslaw and J. C. Jaeger, *Conduction of Heat in Solids*, 2nd Ed. (Oxford University Press, 1959).
- [61] F. Spitzer, Some theorems concerning 2-dimensional Brownian motion, *Trans. Am. Math. Soc.* **87**, 187-197 (1958).

Supplemental Information for the article “Towards a full quantitative description of single-molecule reaction kinetics in biological cells”

I. DETERMINATION OF THE EXPANSION COEFFICIENTS

To compute the coefficients a_n within the self-consistent approximation (SCA), we first substitute $\tilde{S}(r, \theta; p)$ defined in (4) into the modified boundary condition in (3), which gives

$$u'_0(\rho) + \sum_{n=0}^{\infty} a_n g'_n(\rho) \cos(n\theta) = \frac{Q}{R^2} \Theta(\varepsilon - \theta), \quad (\text{S1})$$

where

$$g'_n(r) = \frac{\alpha_n}{L} [I_1(\alpha_n r/L) K_1(\alpha_n R/L) - K_1(\alpha_n r/L) I_1(\alpha_n R/L)]. \quad (\text{S2})$$

Multiplying (S1) by $\cos(n\theta)$ (with $n = 0, 1, 2, \dots$) and integrating over θ from 0 to π , one gets

$$Q = \frac{\pi R^2}{\varepsilon} (u'_0(\rho) + a_0 g'_0(\rho)), \quad (\text{S3})$$

$$a_n = \frac{2Q}{\pi R^2 g'_n(\rho)} \frac{\sin n\varepsilon}{n} \quad (n = 1, 2, \dots), \quad (\text{S4})$$

so that

$$a_n = 2 \frac{u'_0(\rho) + a_0 g'_0(\rho)}{g'_n(\rho)} \frac{\sin n\varepsilon}{n\varepsilon} \quad (n = 1, 2, \dots). \quad (\text{S5})$$

Consequently, $\tilde{S}(r, \theta; p)$ writes

$$\tilde{S}(r, \theta; p) = \frac{R^2}{D} \left(u_0(r) + a_0 g_0(r) + 2(u'_0(\rho) + a_0 g'_0(\rho)) \sum_{n=1}^{\infty} \frac{g_n(r)}{g'_n(\rho)} \frac{\sin n\varepsilon}{n\varepsilon} \cos(n\theta) \right). \quad (\text{S6})$$

The coefficient a_0 (and hence, the trial current Q) remains a free parameter which is to be chosen in a self-consistent way. Within the SCA proposed in [37] (see also [28, 38] for more details on the adaption of this scheme to the first-passage phenomena) the closure relation is obtained by requiring that the mixed boundary condition in (2) holds not locally but *on average*.

For this purpose, we substitute this expression into (2) and integrate the resulting expression over θ from 0 to ε to get

$$a_0 = \frac{1 - \eta}{s g_0(\rho)}, \quad (\text{S7})$$

with η defined by (8). Combining these results, we get an approximate but explicit solution

$$\tilde{S}(r, \theta; p) = \frac{1}{p} \left(1 - \eta \frac{g_0(r)}{g_0(\rho)} + 2\eta \frac{g'_0(\rho)}{g_0(\rho)} \sum_{n=1}^{\infty} \frac{g_n(r)}{g'_n(\rho)} \frac{\sin n\varepsilon}{n\varepsilon} \cos(n\theta) \right), \quad (\text{S8})$$

from which (7) follows.

II. NUMERICAL VALIDATION OF THE RESULTS OBTAINED WITHIN THE SCA

The proposed SCA provides an exact solution of the modified boundary value problem, in which the mixed Robin-Neumann boundary condition in (2) is substituted by the effective inhomogeneous Neumann condition in (3). To check the accuracy of this approximation and hence, of the resulting FPT distribution, we solve the original modified Helmholtz equation by a finite elements method (FEM) implemented in Matlab's PDEtool. Setting $\tilde{H}(r, \theta; p) = u(r/R, \theta; pR^2/D)$ we rewrite the modified Helmholtz equation in cylindrical coordinates as

$$(\partial/\partial r)r(\partial/\partial r)u + r\pi^2(R^2/L^2)(\partial^2/\partial\theta^2)u - rsu = 0, \quad (\text{S9})$$

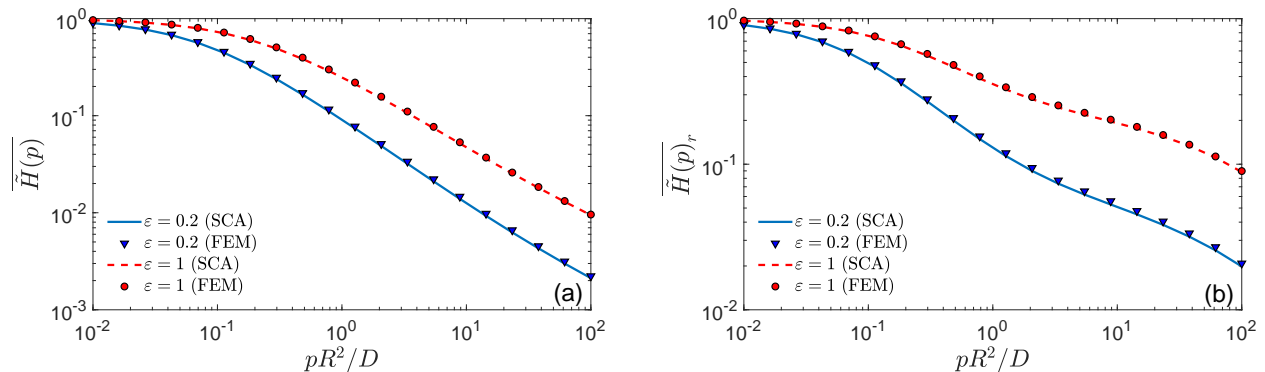


FIG. S1: Volume-averaged **(a)** and surface-averaged **(b)** Laplace-transformed FPT densities $\overline{\tilde{H}(p)}$ and $\overline{\tilde{H}(p)}_r$ as function of $s = pR^2/D$ for $L/R = \pi$, $\rho/R = 0.1$, $r/R = 0.2$, $\kappa = \infty$, and two values of ϵ indicated in the plot. Lines show (10) **(a)** and (11) **(b)** of our self-consistent approximation, in which the series in (9) is truncated to $N = 100$ terms. Symbols present a FEM numerical solution of the modified Helmholtz (S9), with mixed boundary condition (S10) with the maximal mesh size $h = 0.005$. Length and time scales are fixed by setting $R = 1$ and $R^2/D = 1$.

which has to be solved on the rectangular domain $(\rho/R, 1) \times (0, \pi)$ with Neumann boundary condition imposed everywhere except for the segment $(\rho) \times (0, \epsilon)$, for which (2) reads

$$\left(u - \frac{D}{R\kappa} \frac{\partial u}{\partial r} \right) \Big|_{r=\rho} = 1 \quad (0 < \theta < \epsilon). \quad (\text{S10})$$

Once the solution \underline{u} is found on mesh vertices, one can also compute its volume and surface averages. The volume-averaged quantity $\overline{\tilde{H}(p)}$ is obtained by a numerical integration of the solution over the computation domain, whereas the surface-averaged quantity $\overline{\tilde{H}(p)}_r$ is evaluated by first a linear interpolation of the solution to the vertical line at r and then by a numerical integration over this line.

The accuracy of the numerical solution of this problem and its averages is controlled by the maximal mesh size h , i.e., the largest allowed diameter of triangles of the mesh used to discretise the computational domain. In particular, the maximal mesh size should be much smaller than the length ϵ of the reactive segment. This condition limits the accessible target heights ϵ . In our numerical analysis, we set $h = 0.005$ that results in meshes with more than 200 000 triangles. It should be noted that since the numerical solution should be repeated for many values of p (or s), computations with even larger meshes (and thus smaller h and ϵ) become too time-consuming. Moreover, this long computation also prohibits using the Talbot algorithm for the Laplace inversion. Alternatively, the probability density $H(r, \theta; t)$ in time domain might be computed by solving directly the diffusion equation for the survival probability, but this solution would be even more time-consuming and limited to a relatively narrow range of times. For these reasons, we focus here on a numerical validation of the SCA only in the Laplace domain, i.e., checking the moment-generating function over a wide range of variation of the parameter p of the Laplace transform, instead of the probability density function itself. From a formal viewpoint, this is equivalent to validating the FPT distribution since both quantities are uniquely linked by the Laplace transform.

Figure S1 shows excellent agreement between the result based on the SCA and the FEM solution of the original mixed boundary value problem for $\epsilon = 0.2$ and $\epsilon = 1$ (we do not consider the case $\epsilon = \pi$ for which the SCA yields the exact solution, see Section V of the SI). Moreover, the result of the SCA converges rapidly as the upper summation truncation N of the series in (9) increases. In particular, the results for $N = 50$ (not shown) and $N = 100$ are barely distinguishable. Small deviations at large p can be attributed to (i) inaccuracy of the FEM solution (and the consequent numerical integrations for getting volume and surface averages), and (ii) intrinsic small differences between the original and modified problems. Nevertheless, the quality of the SCA is quite impressive.

The SCA becomes particularly robust for imperfect reactions on the target. Figure S2 compares the SCA to the FEM solution for $\epsilon = 0.2$ and several values of κ . The SCA predictions and FEM solutions are indistinguishable at the logarithmic scale. Lastly, as discussed in Ref. [28], the SCA is generally getting more accurate for smaller target size ϵ , smaller reactivity κ , and for starting points that are not too close to the target. Moreover, it was shown recently in Ref. [45], in which the self-propulsion velocity of catalytically-active colloids was studied by a similar method, that also for an arbitrary ϵ the SCA provides an accurate description and only slightly overestimates the numerical factors.

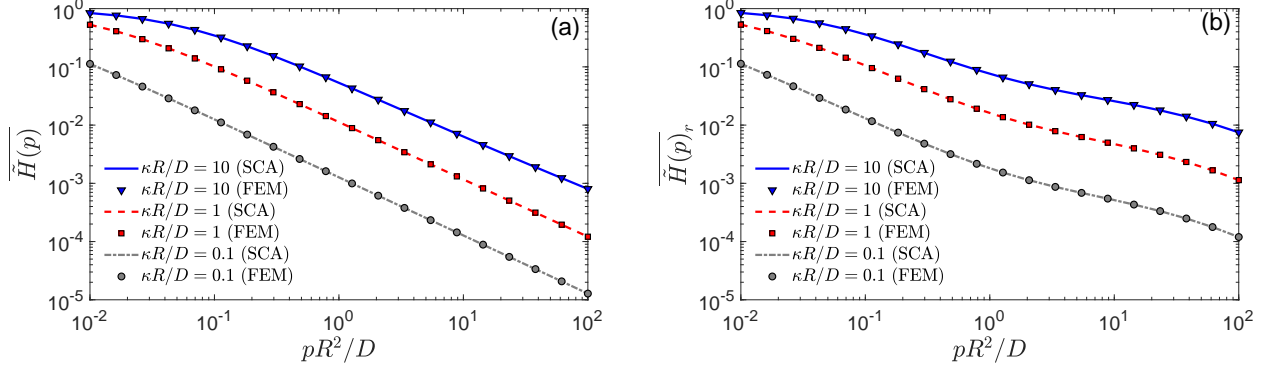


FIG. S2: Volume-averaged (a) and surface-averaged (b) Laplace-transformed FPT densities $\overline{\tilde{H}(p)}$ and $\overline{\tilde{H}(p)}_r$ as function of $s = pR^2/D$ for $L/R = \pi$, $\rho/R = 0.1$, $r/R = 0.2$, $\varepsilon = 0.2$, and three values of κ , indicated in the plot. Lines show (10) (a) and (11) (b) of our self-consistent approximation, in which the series in (9) is truncated to $N = 100$ terms. Symbols present a FEM numerical solution of the modified Helmholtz (S9), with mixed boundary condition (S10) with the maximal mesh size $h = 0.005$. Length and time scales are fixed by setting $R = 1$ and $R^2/D = 1$.

III. THE PROBABILITY DENSITY IN TIME DOMAIN

The Laplace-transformed probability density $\tilde{H}(r, \theta; p)$ and the related surface and volume-averaged quantities can be inverted by using the residue theorem. For this purpose, one searches for the poles of $\tilde{H}(r, \theta; p)$ in the complex plane $p \in \mathbb{C}$. In general, there are two groups of poles, which can be identified as (i) zeros of functions $g'_n(\rho)$ and (ii) zeros of the function $g_0(\rho)/\eta$.

(i) Introducing the auxiliary function

$$\hat{G}(z) \equiv -iz \left(I_1(-iz\rho/R)K_1(-iz) - K_1(-iz\rho/R)I_1(-iz) \right) = -\frac{\pi i}{2} z \left(Y_1(z\rho/R)J_1(z) - J_1(z\rho/R)Y_1(z) \right), \quad (\text{S11})$$

one writes $g'_n(\rho) = \hat{G}(i\alpha_n R/L)/R$, where $\alpha_n = \sqrt{\pi^2 n^2 + pL^2/D}$. One can check that the function $\hat{G}(z)$ has infinitely many zeros all lying on the real axis. Since the Bessel functions obey

$$\begin{aligned} J_n(-x) &= (-1)^n J_n(x) \\ Y_n(-x) &= (-1)^n (Y_n(x) + 2iJ_n(x)) \end{aligned} \quad (x > 0),$$

one deduces that $\hat{G}(-z) = -\hat{G}(z)$. We can thus focus only on the positive zeros of $\hat{G}(z)$ denoted as \hat{z}_k (with $k = 1, 2, \dots$). We relate them to the zeros of $g'_n(\rho)$:

$$p_{n,k} = -D \left(\frac{\hat{z}_k^2}{R^2} + \frac{\pi^2 n^2}{L^2} \right), \quad \begin{pmatrix} n = 1, 2, \dots \\ k = 1, 2, \dots \end{pmatrix}. \quad (\text{S12})$$

For each n , all the poles $p_{n,1}, p_{n,2}, \dots$ are expected to be simple. In turn, it is possible to tune R and L to make some poles with different n coincide and thus be of the order higher than 1. At such poles, the computation of the residue would be more involved.

(ii) Similarly, we introduce the function

$$G_r(z) \equiv I_0(-izr/R)K_1(-iz) + K_0(-izr/R)I_1(-iz) = \frac{\pi i}{2} \left(Y_0(zr/R)J_1(z) - J_0(zr/R)Y_1(z) \right), \quad (\text{S13})$$

to write $g_n(r) = G_r(i\alpha_n R/L)$. Note that this function is also antisymmetric: $G_r(-z) = -G_r(z)$. The poles of the function

$$\frac{\eta}{g_0(\rho)} = \frac{1}{g_0(\rho) - \left(\frac{\pi D}{\kappa \varepsilon} + \frac{L}{\pi} \mathcal{R}_\varepsilon \right) g'_0(\rho)}$$

are related to the zeros of the function

$$F(z) \equiv G_\rho(z) - \left(\frac{\pi D}{R\kappa\varepsilon} + \frac{L}{\pi R} \mathcal{R}_\varepsilon(z) \right) \hat{G}(z), \quad (\text{S14})$$

where

$$\mathcal{R}_\varepsilon(z) = -\frac{2\pi R}{L} \sum_{n=1}^{\infty} \left(\frac{\sin n\varepsilon}{n\varepsilon} \right)^2 \frac{G_\rho(\sqrt{z^2 - \pi^2 n^2 R^2/L^2})}{\hat{G}(\sqrt{z^2 - \pi^2 n^2 R^2/L^2})}. \quad (\text{S15})$$

Denoting the positive zeros of $F(z)$ as z_k , we get the poles as

$$p_{0,k} = -\frac{D}{R^2} z_k^2 \quad (k = 1, 2, \dots). \quad (\text{S16})$$

Having identified all the poles, one can formally invert the Laplace transform by applying the residue theorem.

IV. LONG AND SHORT TIME ASYMPTOTICAL BEHAVIOUR OF THE FPT DENSITY

We here summarise the relations relevant for the calculation of the asymptotic behaviours of the FPT density.

Long-time behaviour

With $p \rightarrow 0$ we also have $s \rightarrow 0$, which then leads to $\alpha_n = \pi n + O(s)$ for $n > 0$ and $\alpha_0 = \sqrt{s}L/R$. We get

$$g_0(r) \simeq \frac{1}{\sqrt{s}} \left(1 + s \left(\frac{r^2}{4R^2} - \frac{1}{2} \ln(r/R) \right) + O(s^2) \right), \quad (\text{S17})$$

so that

$$\frac{g_0(r)}{g_0(\rho)} \simeq 1 - \left(\frac{\rho^2 - r^2}{4R^2} + \frac{\ln(r/\rho)}{2} \right) s + O(s^2), \quad (\text{S18})$$

$$\frac{g'_0(\rho)}{g_0(\rho)} \simeq -s \frac{1 - (\rho/R)^2}{2\rho} + O(s^2), \quad (\text{S19})$$

$$\mathcal{R}_\varepsilon \simeq \mathcal{R}_\varepsilon(p=0) + O(s), \quad (\text{S20})$$

$$\eta^{-1} \simeq 1 + p\bar{T}_\rho + O(p^2), \quad (\text{S21})$$

where \bar{T}_ρ from (14) is the surface-averaged MFPT studied in Ref. [38].

Short-time behaviour

The short-time behaviour corresponds to the limit $p \rightarrow \infty$, in which we get

$$\frac{g_n(\rho)}{g'_n(\rho)} \simeq -\frac{L}{\alpha_n} \frac{K_0(\alpha_n \rho/L)}{K_1(\alpha_n \rho/L)} \simeq -\frac{L}{\alpha_n} \left(1 - \frac{1}{2\alpha_n \rho/L} + \frac{3}{8(\alpha_n \rho/L)^2} + \dots \right) \quad (\text{S22})$$

and

$$\mathcal{R}_\varepsilon \simeq 2\pi \sum_{n=1}^{\infty} \left(\frac{\sin n\varepsilon}{n\varepsilon} \right)^2 \left(\frac{1}{\alpha_n} - \frac{L}{2\rho\alpha_n^2} + \dots \right). \quad (\text{S23})$$

Setting $z = \sqrt{s}L/R$ we identify the leading part in the first term by writing

$$\mathcal{R}_\varepsilon \simeq 2\pi \sum_{n=1}^{\infty} \left(\frac{\sin n\varepsilon}{n\varepsilon} \right)^2 \left(\frac{1}{z} - \frac{\pi^2 n^2}{z\alpha_n(\alpha_n + z)} - \frac{L}{2\rho\alpha_n^2} + \dots \right). \quad (\text{S24})$$

The first term yields the leading contribution equal to $\frac{\pi(\pi-\varepsilon)}{\varepsilon} z^{-1}$, in virtue of the identity

$$\sum_{n=1}^{\infty} \left(\frac{\sin n\varepsilon}{n\varepsilon} \right)^2 = \frac{\pi - \varepsilon}{2\varepsilon}. \quad (\text{S25})$$

The second sum in (S24) can be written as

$$\mathcal{R}_\varepsilon^{(2)} = -\frac{\pi^3}{z\varepsilon^2} \sum_{n=1}^{\infty} \frac{1 - \cos 2n\varepsilon}{\pi^2 n^2 + z^2 + \alpha_n z} \simeq -\frac{\pi^3}{z\varepsilon^2} \sum_{n=1}^{\infty} \frac{1 - \cos 2n\varepsilon}{\pi^2 n^2 + 2z^2}, \quad (\text{S26})$$

where we substituted $\alpha_n \simeq z$ (for large z) in the denominator of the last term. Using the identity

$$\sum_{n=1}^{\infty} \frac{\cos(\pi n x)}{\pi^2 n^2 + z^2} = \frac{\cosh(1-x)z}{2z \sinh z} - \frac{1}{2z^2}, \quad (\text{S27})$$

which is valid for $0 \leq x \leq 1$, we find

$$\mathcal{R}_\varepsilon^{(2)} \simeq -\frac{\pi^3}{z\varepsilon^2} \frac{\cosh(z\sqrt{2}) - \cosh(z\sqrt{2}(1 - 2\varepsilon/\pi))}{2\sqrt{2}z \sinh(z\sqrt{2})}. \quad (\text{S28})$$

We emphasise that this relation is only valid for $\varepsilon \leq \pi/2$. At large s (or z), one thus gets a very accurate approximation

$$\mathcal{R}_\varepsilon^{(2)} \simeq -\frac{\pi^3}{2\sqrt{2}z^2\varepsilon^2} (1 - e^{-2\sqrt{2}z\varepsilon/\pi}). \quad (\text{S29})$$

Finally, in the third term of (S24) we approximate again $\alpha_n^2 \approx z^2$, which yields $-\frac{\pi(\pi-\varepsilon)L}{2\varepsilon\rho}z^{-2}$. Combining these results, we obtain

$$\mathcal{R}_\varepsilon \simeq \frac{\pi(\pi-\varepsilon)R}{\varepsilon L} s^{-1/2} - \mathcal{A} s^{-1} + O(s^{-3/2}), \quad (\text{S30})$$

with

$$\mathcal{A} = \frac{\pi R^2}{\varepsilon L^2} \left(\frac{\pi^2}{2\sqrt{2}\varepsilon} + \frac{(\pi-\varepsilon)L}{2\rho} \right), \quad (\text{S31})$$

in which we neglected the exponential correction in (S29).

From (S22), we also get

$$-\frac{g'_0(\rho)}{g_0(\rho)} \simeq \frac{\sqrt{s}}{R} + \frac{1}{2\rho} - \frac{R}{8\rho^2} s^{-1/2} + O(s^{-1}). \quad (\text{S32})$$

Combining these results, we find the large s asymptotic behaviour of (8),

$$\eta \simeq \frac{\varepsilon}{\pi} \left[s^{1/2} \frac{D}{\kappa R} + \left(1 + \frac{D}{2\kappa\rho} \right) - \left(\frac{DR}{8\kappa\rho^2} + \frac{\pi R}{\sqrt{8}\varepsilon L} \right) s^{-1/2} + O(s^{-1}) \right]^{-1}. \quad (\text{S33})$$

When $\kappa = \infty$, (S33) becomes

$$\eta \simeq \frac{\varepsilon}{\pi} + \frac{\sqrt{D}}{2\sqrt{2}L} p^{-1/2} + O(p^{-1}). \quad (\text{S34})$$

When the particles start from a cylindrical surface at r , to obtain (18) we need the large- s asymptotic relation

$$g_0(r) \simeq \frac{\cosh(\sqrt{s}(1 - \frac{r}{R}))}{\sqrt{s}\sqrt{r/R}} \left(1 - \frac{\tanh(\sqrt{s}(1 - \frac{r}{R}))}{8} (3 + R/r) s^{-1/2} + O(s^{-1}) \right), \quad (\text{S35})$$

from which we find the Laplace-transformed FTP density

$$\overline{H(p)}_r \simeq \eta \sqrt{\rho/r} \exp(-(r-\rho)\sqrt{p/D}) \left(1 + \sqrt{D} \frac{\sqrt{R/\rho} - \sqrt{R/r}}{8R} p^{-1/2} + O(p^{-1}) \right) \quad (\text{S36})$$

for $r < R$ and $p \rightarrow \infty$.

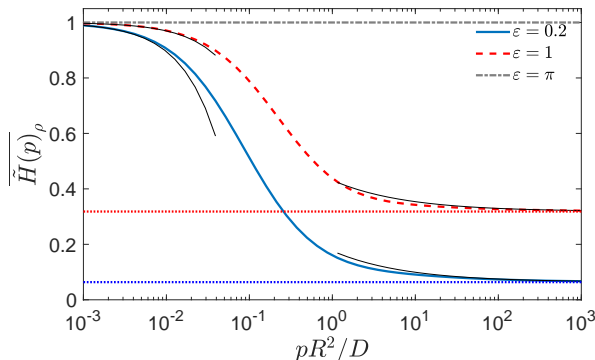


FIG. S3: Surface-averaged Laplace-transformed FPT density $\overline{\tilde{H}(p)}_\rho$ as function of $s = pR^2/D$ for $L/R = \pi$, $\rho/R = 0.1$, $\kappa = \infty$, and the three values of ϵ indicated in the plot. Thin solid lines show the asymptotic (S21) and (S34) as $s \rightarrow 0$ and $s \rightarrow \infty$, respectively. Dotted horizontal lines indicate the asymptotic limit ϵ/π of the FPT density as $s \rightarrow \infty$. Length and time scales are fixed by setting $R = 1$ and $R^2/D = 1$.

For $\kappa < \infty$, (S33) becomes

$$\eta \simeq \frac{\epsilon}{\pi} \frac{\kappa}{\sqrt{D}} p^{-1/2} - \frac{\epsilon}{\pi} \left(\frac{\kappa^2}{D} + \frac{\kappa}{2\rho} \right) p^{-1} + O(p^{-3/2}), \quad (\text{S37})$$

which leads to (20).

Figure S3 illustrates the behaviour of the surface-averaged probability density $\overline{\tilde{H}(p)}_\rho$ for three target heights ϵ in the case of perfect reactions ($\kappa = \infty$). We observe that $\overline{\tilde{H}(p)}_\rho$ linearly approaches unity as $p \rightarrow 0$ (see (S21)) and reaches a constant ϵ/π , that is, the fraction of the target area, as $p \rightarrow \infty$. This is a consequence of the uniform surface average: particles that start from the target are immediately absorbed and thus not affected by diffusion-reaction processes. The case $\epsilon = \pi$ corresponds to the fully absorbing inner cylinder, with $\overline{\tilde{H}(p)}_\rho = \eta = 1$.

V. TARGET ON THE WHOLE INNER CYLINDER

We consider the special case of the target extended to the whole inner cylinder (i.e., $\epsilon = \pi$), for which $a_n = 0$ ($n > 0$), $\mathcal{R}_\pi = 0$, and thus the SCA yields

$$\tilde{S}(r, \theta; p) = \frac{1}{p} \left(1 - \eta \frac{g_0(r)}{g_0(\rho)} \right), \quad (\text{S38})$$

with

$$\eta = \left(1 - \frac{g'_0(\rho)}{g_0(\rho)} \frac{D}{\kappa} \right)^{-1}. \quad (\text{S39})$$

One can easily check that this is the *exact* solution of the original problem with a partially absorbing inner cylinder, i.e., this function satisfies the Robin boundary condition at $r = \rho$:

$$(D\partial_n \tilde{S} + \kappa \tilde{S})_{r=\rho} = 0. \quad (\text{S40})$$

In other words, our approximation becomes exact in the case $\epsilon = \pi$.

From (S38), we also get the MFPT to the inner cylinder:

$$T = \frac{R^2 - \rho^2}{2\rho\kappa} + \frac{\rho^2 - r^2}{4D} + \frac{R^2 \ln(r/\rho)}{2D}, \quad (\text{S41})$$

whereas its volume average reads

$$\overline{T} = \frac{R^2 - \rho^2}{2\rho\kappa} + \frac{R^2}{8D} \left(\frac{4 \ln(R/\rho)}{1 - (\rho/R)^2} - 3 + (\rho/R)^2 \right). \quad (\text{S42})$$

The above exact solution suggests an interesting interpretation of the coefficient \mathcal{R}_ε for the general case of an arbitrary ε . In fact, when the reactive region is only a part of the inner cylinder (i.e., $\varepsilon < \pi$), a diffusing particle will undergo multiple reflections by the remaining part of the inner cylinder until it reaches the target. If the target was composed of many small regions uniformly distributed over the inner cylinder, such a partially reactive boundary could be described by the Robin boundary condition over the whole inner cylinder, with an effective reactivity κ_{eff} . In our case, the target is a single absorbing region, so that this homogenisation argument is *a priori* not applicable. Nevertheless, one can still introduce an effective, *apparent* reactivity by looking at the form of η in (8):

$$\frac{\pi}{\kappa\varepsilon} + \frac{L}{\pi D}\mathcal{R}_\varepsilon = \frac{1}{\kappa_{\text{eff}}}. \quad (\text{S43})$$

This relation can be thought of as an extension of the celebrated Collins-Kimball relations for the system under study (see [28, 38] for more details).

When the target is perfectly reactive, $\kappa = \infty$ and thus the effective reactivity represents the effect of the mixed Dirichlet-Neumann boundary condition: $\kappa_{\text{eff}} = \frac{D\pi}{L\mathcal{R}_\varepsilon}$. If in addition the target is partially reactive, the overall reactivity is further reduced, as the particle has to reach the reactive part and then overcome the energy barrier. Interpreting the inverse of the reactivity as a “resistance”, (S43) implies that the respective resistances enter additively, precisely as it happens in the classic analysis of Collins and Kimball.

VI. THE LIMIT $R \rightarrow \infty$

The distribution of the FPT remains well defined in the limit $R \rightarrow \infty$ when the outer cylinder moves to infinity. However, the MFPT diverges in this limit.

We get $\alpha_n = \sqrt{\pi^2 n^2 + pL^2/D}$, and $g_n(r) \simeq K_0(\alpha_n r/L)I_1(\alpha_n R/L)$, with an exponentially large factor $I_1(\alpha_n R/L)$. In particular, one finds

$$\tilde{S}_0(r;p) = \frac{1}{p} \left(1 - \frac{K_0(r\sqrt{p/D})}{K_0(\rho\sqrt{p/D})} \right) \quad (\text{S44})$$

and

$$\frac{g_n(r)}{g'_n(\rho)} = -\frac{L}{\alpha_n} \frac{K_0(\alpha_n r/L)}{K_1(\alpha_n \rho/L)}. \quad (\text{S45})$$

As a consequence, the Laplace-transformed pdf from (7) becomes

$$\tilde{H}(r, \theta; p) = \eta \frac{K_0(r\sqrt{p/D})}{K_0(\rho\sqrt{p/D})} + 2\eta L\sqrt{p/D} \frac{K_1(\rho\sqrt{p/D})}{K_0(\rho\sqrt{p/D})} \sum_{n=1}^{\infty} \frac{K_0(\alpha_n r/L)}{\alpha_n K_1(\alpha_n \rho/L)} \frac{\sin n\varepsilon}{n\varepsilon} \cos(n\theta), \quad (\text{S46})$$

where

$$\eta^{-1} = 1 + \left(\frac{\pi D}{\kappa\varepsilon} + \frac{L}{\pi}\mathcal{R}_\varepsilon \right) \frac{\sqrt{p/D} K_1(\rho\sqrt{p/D})}{K_0(\rho\sqrt{p/D})} \quad (\text{S47})$$

and

$$\mathcal{R}_\varepsilon = 2\pi \sum_{n=1}^{\infty} \frac{K_0(\alpha_n \rho/L)}{\alpha_n K_1(\alpha_n \rho/L)} \left(\frac{\sin n\varepsilon}{n\varepsilon} \right)^2. \quad (\text{S48})$$

In particular, the surface average of (S46) yields

$$\overline{\tilde{H}(p)}_r = \eta \frac{K_0(r\sqrt{p/D})}{K_0(\rho\sqrt{p/D})}, \quad (\text{S49})$$

whereas the volume average in (10) diverges as $R \rightarrow \infty$.

The particular case $\varepsilon = \pi$

The distribution of the FPT has already been studied in the particular case of a perfectly absorbing inner cylinder (i.e., $\varepsilon = \pi$ and $\kappa = \infty$). In this case, $\eta = 1$, and one retrieves the Laplace-transformed pdf of the FPT to a cylinder of radius ρ [61]. In particular, the distribution of the FPT in this particular case is known to be characterised by a power-law tail, $H_\pi(r; t) \propto 1/(t \ln^2(t))$ as $t \rightarrow \infty$, where subscript π signifies that this solution corresponds to $\varepsilon = \pi$, in which the vertical coordinate z (or θ) is irrelevant and thus the surface average does not change the solution. Levitz *et al.* [56] derived an approximation to $H_\pi(r; t)$ over the whole range of times (see below)

$$H_\pi(r; t) \simeq \begin{cases} \frac{r - \rho}{\sqrt{4\pi Dt^3}} \exp\left(-\frac{(r - \rho)^2}{4Dt}\right) & (t < \rho^2/(2D)), \\ \frac{r/\rho - 1}{2t(1 + \rho/\sqrt{2Dt}) \ln^2((r + \sqrt{2Dt})/\rho)} & (t > \rho^2/(2D)). \end{cases} \quad (\text{S50})$$

This approximation is only valid for r close to ρ , i.e., when the particle starts in a vicinity of the inner cylinder.

We consider the more general case of a partially reactive inner cylinder (i.e., $\varepsilon = \pi$ and $\kappa < \infty$), for which (S46) becomes

$$\tilde{H}_\pi(r; p) = \frac{K_0(r\sqrt{p/D})}{K_0(\rho\sqrt{p/D}) + \frac{D}{\kappa}\sqrt{p/D}K_1(\rho\sqrt{p/D})}. \quad (\text{S51})$$

Using the solution of an appropriate heat problem (see Ref. [60], p. 337), we can write the inverse Laplace transform as

$$H_\pi(r; t) = \frac{2\kappa}{\pi} \int_0^\infty dq q e^{-Dtq^2} \frac{Y_0(qr)(qJ_1(q\rho) + hJ_0(q\rho)) - J_0(qr)(qY_1(q\rho) + hY_0(q\rho))}{(qJ_1(q\rho) + hJ_0(q\rho))^2 + (qY_1(q\rho) + hY_0(q\rho))^2}, \quad (\text{S52})$$

where $h = \kappa/D$. In the long-time limit, the main contribution to the integral comes from $q \approx 0$. The asymptotic behaviour of the integrand function at $q \rightarrow 0$ yields

$$H_\pi(r; t) \simeq \frac{2\left(\frac{D}{\rho\kappa} + \ln(r/\rho)\right)}{t} \int_0^\infty \frac{dz e^{-z}}{\pi^2 + \left(-\frac{2D}{\rho\kappa} + \ln(z\rho^2/(4Dt)) + 2\gamma\right)^2}, \quad (\text{S53})$$

where $\gamma \approx 0.5772\dots$ is the Euler constant. Discarding a slowly varying function $\ln(z)$ in the denominator, we find the following long-time asymptotic form

$$H_\pi(r; t) \simeq \frac{2\left(\frac{D}{\rho\kappa} + \ln(r/\rho)\right)}{t\left[\pi^2 + \left(\ln(\rho^2/(4Dt)) + 2\gamma - \frac{2D}{\rho\kappa}\right)^2\right]}, \quad (\text{S54})$$

which exhibits a very slow decrease $1/(t \ln^2(t))$ as $t \rightarrow \infty$.

In the short-time limit, one uses the asymptotic behaviour of the integrand function as $q \rightarrow \infty$ to get

$$H_\pi(r; t) \simeq \frac{2\kappa\sqrt{\rho/r}}{\pi} \int_0^\infty dq q e^{-Dtq^2} \frac{q \cos(q(r - \rho)) + h \sin(q(r - \rho))}{q^2 + h^2}.$$

Ignoring the second term in the numerator, one gets the short-time asymptotic behaviour

$$H_\pi(r; t) \simeq \frac{\kappa\sqrt{\rho/r}}{\sqrt{\pi Dt}} \exp\left(-\frac{(r - \rho)^2}{4Dt}\right) \quad (t \rightarrow 0). \quad (\text{S55})$$

In the limit $\kappa \rightarrow \infty$ (perfect reactions), the exact solution in (S52) and its approximations (S54) and (S55) become respectively

$$H_\pi(r; t) = \frac{2D}{\pi} \int_0^\infty dq q e^{-Dtq^2} \frac{Y_0(qr)J_0(q\rho) - J_0(qr)Y_0(q\rho)}{J_0^2(q\rho) + Y_0^2(q\rho)}, \quad (\text{S56})$$

$$H_\pi(r; t) \simeq \frac{2 \ln(r/\rho)}{t\left[\pi^2 + \left(\ln(\rho^2/(4Dt)) + 2\gamma\right)^2\right]} \quad (t \rightarrow \infty), \quad (\text{S57})$$

$$H_\pi(r; t) \simeq \frac{(r - \rho)\sqrt{\rho/r}}{\sqrt{4\pi Dt^3}} \exp\left(-\frac{(r - \rho)^2}{4Dt}\right) \quad (t \rightarrow 0). \quad (\text{S58})$$

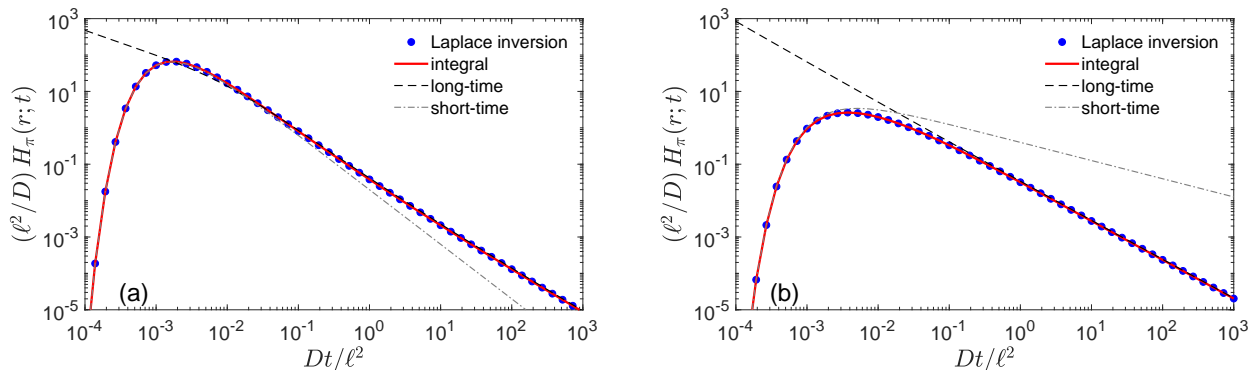


FIG. S4: The probability density $H_\pi(r; t)$ as function of t for $R = \infty$, $L/\ell = \varepsilon = \pi$, $\rho/\ell = 0.1$, $\kappa = \infty$ (a) and $\kappa\ell/D = 1$ (b). The exact integral representation in (S52) (solid line) is compared to the numerical Laplace inversion of (S51) (circles) and to the long-time and short-time approximations (S54) and (S55). Length and time scales are fixed by setting $\ell = 1$ and $\ell^2/D = 1$, with an auxiliary length $\ell = L/\pi$.

As in Ref. [56], one can combine the short-time and long-time approximations to cover the whole range of times. If the maximum of $H_\pi(r; t)$ occurs in the validity range of (S58), one can easily get the most probable FPT by finding the zero of $\partial H_\pi(r; t)/\partial t$: $t_m = (r - \rho)^2/(6D)$. This value is three times smaller than that from (21) for a partially reactive target. The difference in the prefactor comes from different power law corrections to the common exponential function (cf. (S55) and (S58)): $t^{-3/2}$ for the perfectly reactive case and $t^{-1/2}$ for the partially reactive case.

Figure S4 illustrates the behaviour of the probability density $H_\pi(r; t)$. The exact integral representation in (S52) agrees perfectly with the numerical Laplace inversion of (S51) over a very broad range of times, confirming the high accuracy of the inversion procedure. When the inner cylinder is perfectly absorbing ($\kappa = \infty$), the long-time and short-time approximations ((S54) and (S55)) are very accurate and can be used to approximate the probability density over the whole range of times. For a partially reactive cylinder ($\kappa = 1$), these approximations are less accurate but still good.

Comment on the approximation in (S50)

We briefly comment on the approximation in (S50) derived in Ref. [56]:

(i) we note that Eq. (1) in Ref. [56] is incorrect: the numerator and the denominator should be inter-changed. This typing error does not impact the consequent results.

(ii) the approximate Eq. (6) in Ref. [56] was derived under the simplifying assumption that the distance from the cylinder, $\delta = r - \rho$, is much smaller than the radius of the cylinder ρ . The same derivation without this assumption yields

$$H_\pi(r; t) = \frac{\ln(r/\rho)}{2t(1 + r/\sqrt{2Dt}) \ln^2((r + \sqrt{2Dt})/\rho)}. \quad (\text{S59})$$

When $\delta \ll \rho$, one has $\ln(r/\rho) = \ln(1 + \delta/\rho) \simeq r/\rho - 1$, and thus retrieves (S50), with r replaced by ρ in the denominator. As pointed out in Ref. [56], the approximation $H_\pi(r; t)$ has the correct normalisation by construction:

$$\int_0^\infty dt H_\pi(r; t) = 1. \quad (\text{S60})$$

Since this approximation is only valid for long times, it can be completed by the short-time behaviour.

(iii) the approximation in (S50) and its extension in (S59) are slightly different from our asymptotic (S57) but they become identical in the long-time limit.

VII. THE LIMIT $L \rightarrow \infty$

In the limit $L \rightarrow \infty$, the capped annular domain transforms into an unbounded semi-infinite circular annulus: $\Omega = \{\mathbf{x} \in \mathbb{R}^3 : \rho < \sqrt{x^2 + y^2} < R, z > 0\}$. In this case, the discrete summation variable $\xi = \pi n/L$ becomes

continuous, and one can replace sums by integrals. In particular, we get $\alpha_n/L = \sqrt{\xi^2 + p/D}$, and (9) becomes

$$\mathcal{R}_\epsilon = \int_0^\infty d\xi \Upsilon(\rho, \sqrt{\xi^2 + p/D}) \left(\frac{\sin \xi \epsilon}{\xi \epsilon} \right)^2, \quad (\text{S61})$$

with

$$\Upsilon(r, \alpha) = -2 \frac{I_0(\alpha r) K_1(\alpha R) + K_0(\alpha r) I_1(\alpha R)}{\alpha (I_1(\alpha \rho) K_1(\alpha R) - K_1(\alpha \rho) I_1(\alpha R))}. \quad (\text{S62})$$

Since (8) yields

$$\eta \simeq -\frac{\pi g_0(\rho)}{L g'_0(\rho)} \left(\frac{\pi D}{\kappa \epsilon} + \mathcal{R}_\epsilon \right)^{-1}, \quad (\text{S63})$$

the first term in (7) vanishes, whereas the second term transforms into

$$\tilde{H}(r, z; p) = \left(\frac{\pi D}{\kappa \epsilon} + \mathcal{R}_\epsilon \right)^{-1} \int_0^\infty d\xi \Upsilon(r, \sqrt{\xi^2 + p/D}) \frac{\sin \xi \epsilon}{\xi \epsilon} \cos \xi z. \quad (\text{S64})$$

Due to the symmetry, this solution is also valid for an infinite circular annulus with the target region $(-\epsilon, \epsilon)$ on the inner cylinder. Note also that in the second limit $R \rightarrow \infty$, the function Υ reads

$$\Upsilon(r, \alpha) = \frac{2K_0(\alpha r)}{\alpha K_1(\alpha \rho)}. \quad (\text{S65})$$

It is instructive to evaluate $\tilde{H}(r, z; p = 0)$, which corresponds to the normalisation of the FPT. For a finite R , the integrals in (S61) and (S64) diverge as $p \rightarrow 0$, implying $\tilde{H}(r, z; p = 0) = 1$, as expected. In contrast, when $R = \infty$, both integrals are finite, and thus $\tilde{H}(r, z; p = 0) < 1$, i.e., the density $H(r, z; t)$ is not normalised to 1. This is the consequence of the transient character of the search process in three dimensions (when $L = R = \infty$). In this setting, $\tilde{H}(r, z; p = 0)$ is the probability of finding the target.

In the limit $p \rightarrow \infty$, we have

$$\Upsilon(r, \alpha) \simeq \frac{2\sqrt{\rho/r}}{\alpha} e^{-\alpha(r-\rho)} \quad (\text{S66})$$

so that

$$\mathcal{R}_\epsilon \simeq \frac{\pi}{\epsilon \sqrt{p/D}}. \quad (\text{S67})$$

For $0 < z < \epsilon$, we evaluate the leading contribution to the integral in (S64) and get

$$\tilde{H}(r, z; p) \simeq \sqrt{\rho/r} \frac{e^{-(r-\rho)\sqrt{p/D}}}{1 + \sqrt{p/D}/\kappa}, \quad (\text{S68})$$

which does not depend on ϵ and R in the leading order. Inverting this relation, we get the short-time asymptotic behaviour

$$H(r, z; t) \simeq \sqrt{\rho/r} e^{-(r-\rho)^2/(4Dt)} \left\{ \frac{\kappa}{\sqrt{\pi Dt}} - \frac{\kappa^2}{D} \operatorname{erfcx} \left(\left(\frac{r-\rho}{\sqrt{4Dt}} + \frac{\kappa\sqrt{t}}{\sqrt{D}} \right)^2 \right) \right\}, \quad (\text{S69})$$

where $\operatorname{erfcx}(x) = e^{x^2} \operatorname{erfc}(x)$ is the scaled complementary error function. In the perfectly reactive case $\kappa = \infty$, this expression is reduced to

$$H(r, z; t) \simeq \sqrt{\rho/r} \frac{r-\rho}{\sqrt{4\pi Dt^3}} e^{-(r-\rho)^2/(4Dt)}. \quad (\text{S70})$$

In the case $z \geq \epsilon$, the integral in (S64) requires a more subtle evaluation that we do not discuss here.

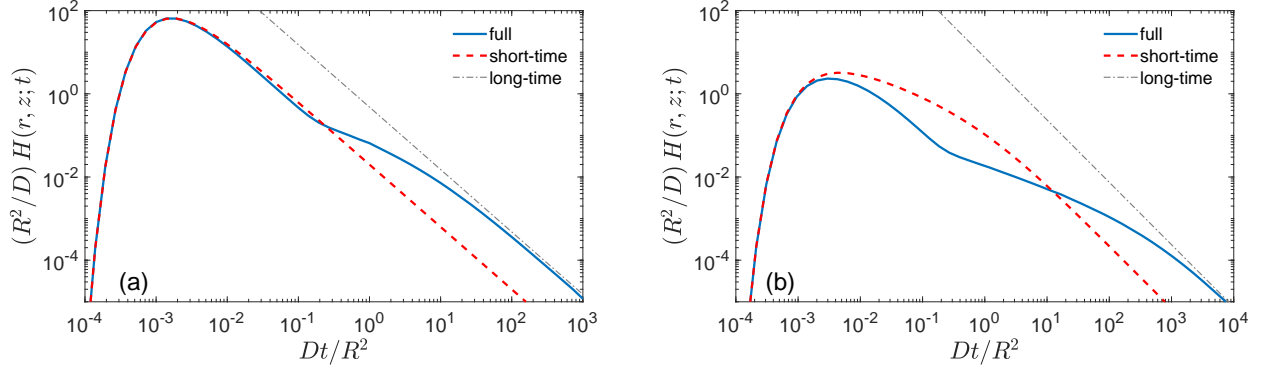


FIG. S5: The probability density $H(r, z; t)$ as function of t for $L = \infty$, $\epsilon/R = 0.2$, $z/R = 0.1$, $\rho/R = 0.1$, $r/R = 0.2$, $\kappa = \infty$ (a) and $\kappa R/D = 1$ (b). The numerical Laplace inversion of the integral representation in (S64) (solid line) is compared to its short-time behaviour (dashed line) in (S69) (for $\kappa R/D = 1$) and (S70) (for $\kappa = \infty$) and long-time asymptotic relation in (S76) (dash-dotted line). Length and time scales are fixed by setting $R = 1$ and $R^2/D = 1$.

In the opposite limit $p \rightarrow 0$, the major contribution to integrals comes from $\xi \approx 0$. Since

$$\Upsilon(r, \alpha) \simeq \frac{4\rho}{\alpha^2(R^2 - \rho^2)} + \frac{2\rho}{R^2 - \rho^2} Y_r \quad (\alpha \rightarrow 0), \quad (\text{S71})$$

with

$$Y_r = \frac{r^2 - R^2}{2} - \frac{R^2 + \rho^2}{4} + R^2 \ln(R/r) + \frac{R^2 \rho^2 \ln(R/\rho)}{R^2 - \rho^2}, \quad (\text{S72})$$

we deduce the leading contribution to \mathcal{R}_ϵ

$$\mathcal{R}_\epsilon \simeq \frac{2\pi\rho}{(R^2 - \rho^2)\sqrt{p/D}} + \frac{\pi\rho Y_\rho}{\epsilon(R^2 - \rho^2)}. \quad (\text{S73})$$

Similarly, we get for $0 < z < \epsilon$

$$\int_0^\infty d\xi \Upsilon(r, \sqrt{\xi^2 + p/D}) \frac{\sin \xi \epsilon}{\xi \epsilon} \cos \xi z \simeq \frac{2\pi\rho}{(R^2 - \rho^2)\sqrt{p/D}} + \frac{\pi\rho Y_r}{\epsilon(R^2 - \rho^2)}, \quad (\text{S74})$$

from which

$$\tilde{H}(r, z; p) \simeq 1 - \sqrt{p/D} \frac{1}{2\epsilon} \left(\frac{D}{\kappa\rho} (R^2 - \rho^2) + \frac{\rho^2 - r^2}{2} + R^2 \ln(r/\rho) \right), \quad (\text{S75})$$

from which we deduce the long-time asymptotic behaviour

$$H(r, z; t) \simeq \frac{1}{\sqrt{4\pi Dt^3}} \frac{1}{2\epsilon} \left(\frac{D}{\kappa\rho} (R^2 - \rho^2) + \frac{\rho^2 - r^2}{2} + R^2 \ln(r/\rho) \right). \quad (\text{S76})$$

We retrieved the characteristic $t^{-3/2}$ decay of the FPT density for one-dimensional Brownian motion, which is supplemented by the geometric information on the target and the annular domain.

Figure S5 illustrates the probability density $H(r, z; t)$ as function of t for a semi-infinite circular annulus. One can see that both short-time and long-time asymptotic relations accurately capture this behaviour at small and large t , respectively.